
Learning When to Adapt

Ali Zindari^{1,2} Xiaowen Jiang^{1,2} Rotem Mulayoff² Sebastian U. Stich²
¹Universität des Saarlandes ²CISPA Helmholtz Center for Information Security
Saarbrücken, Germany
{ali.zindari,xiaowen.jiang,rotem.mulayoff,stich}@cispa.de

Abstract

Low-rank adaptation (LORA) is a widely used parameter-efficient fine-tuning method, yet its learned correction is static: the same low-rank update is applied to every input. This input-agnostic approach creates an inevitable compromise between adapting to the fine-tuning distribution and preserving pre-trained behavior on inputs outside that distribution, contributing to *catastrophic forgetting*. We introduce DISeL (**D**ynamic **I**nter-sensitive **L**oRA), which augments LORA modules with lightweight input-dependent gates over individual rank-one components. The gating mechanism is designed to preserve the pre-trained model’s behavior by default, while training learns to activate selected components that reduce the fine-tuning loss. DISeL adds only a small number of parameters and preserves the low-rank structure. Across ROBERTa on GLUE, and LLAMA and MISTRAL models fine-tuned for mathematical reasoning and code generation, DISeL reduces forgetting relative to LoRA and related variants while maintaining competitive fine-tuning accuracy. In addition, the learned gate activations provide an interpretable diagnostic view of which layers and rank components are most activated during fine-tuning, giving insight into where task-specific adaptation is concentrated. Code available at: <https://github.com/alizindari/DISeL>.

1 Introduction

Fine-tuning (FT) has become a central stage in the deployment of large language models (LLMs) where pre-trained models with general knowledge are specialized for instruction-following [37, 54], mathematical reasoning [59, 60], code generation [31, 40], and other downstream tasks. The most direct approach is *full fine-tuning*, which updates all parameters of the pre-trained model without constraint. Parameter-efficient fine-tuning (PEFT) methods instead restrict updates to a smaller, structured subspace. The most popular approach is Low-Rank Adaptation (LORA) [19], which freezes the pre-trained weights and learns a low-rank correction using matrix factorization.

Despite achieving strong performance on their target tasks, fine-tuned models often exhibit degradation in their broader capabilities acquired during pre-training [13, 30]. This phenomenon, known as *catastrophic forgetting*, has been frequently studied in continual learning [27, 33, 48, 49, 51] and remains a key challenge in modern LLM fine-tuning. The extent of forgetting depends on the choice of fine-tuning method. Typically, full fine-tuning incurs substantial performance degradation outside the fine-tuning domain [2, 30], whereas LORA mitigates this effect but does not eliminate it [2, 42].

The main reason for forgetting in these FT methods is that the learned modification is input-agnostic. Full fine-tuning, LORA, and its variants such as DORA [28] and ADALORA [62] only differ in parameterization. Yet, they all apply a constant modification across the entire input space, regardless of whether correction is required. As a result, the same adaptation affects both fine-tuning-domain inputs, where correction is needed, and pre-training-domain inputs, where the original mapping should be preserved. This leads to an inherent compromise between adaptation and retention.

Existing input-dependent adaptations are primarily designed to mitigate interference across tasks or among multiple LORA modules. For instance, mixture-of-LORA approaches [4, 45, 58] learn routing or gating mechanisms that select or combine multiple LORA modules based on the input. The closest to this work is GATED LORA [15], which introduces for each rank-one-component, an input-dependent gate within a single adapter. However, its primary goal is to reduce inter-task interference in multi-task fine-tuning, rather than to preserve pre-trained behavior. None of the current methods explicitly target catastrophic forgetting, nor are they designed to make the adapter inactive on inputs outside the fine-tuning distribution, a key property for preserving pre-trained capabilities.

To this end, we propose DISeL (**D**ynamic **I**ntput-**S**ensitive **L**o**R**A), which preserves the low-rank parameterization of LORA but makes the correction input-dependent and active only when necessary. The key idea is to multiply each rank-one component by an input-dependent learnable gate whose output lies in $[0, 1]$. The gates are effectively pre-set to zero in initialization, meaning that DISeL begins training with the pre-trained model. During training, gates are activated only when doing so reduces the fine-tuning loss, leading to updates that are applied selectively across inputs rather than uniformly. The computational overhead for training relative to existing methods is negligible, while the inference cost matches that of LORA, making DISeL a practical alternative.

Contributions. In this work, we introduce an FT method that minimizes forgetting while maintaining strong performance on the fine-tuning task. Specifically, we make the following contributions.

- We identify the input-agnostic nature of full fine-tuning/LORA modifications as a contributing factor in catastrophic forgetting, and illustrate this in a minimal linear regression setting (Sec. 2).
- We introduce DISeL, which augments each LORA module with lightweight, input-dependent gates that activate only when needed, at negligible parameter and compute overhead (Sec. 3).
- We conduct experiments on LLAMA and MISTRAL models fine-tuned for mathematical reasoning and code generation. DISeL consistently reduces catastrophic forgetting compared with LORA and its variants, while maintaining competitive in-domain accuracy (Sec. 4).
- The learned gate activations reveal which layers are most engaged during fine-tuning, providing direct insight into where task-specific knowledge is localized within the network (Sec. 5).

2 Background and motivation

Fine-tuning. Let \mathbf{W}_0 denote the parameters of a pre-trained model. Standard fine-tuning methods learn an additive update of the form

$$\mathbf{W} = \mathbf{W}_0 + \Delta. \quad (1)$$

Depending on the method, Δ can have a specific structure. Full FT [11, 37] updates the entire parameter set \mathbf{W} without constraints, incurring high memory overhead and often increasing susceptibility to forgetting [2]. In contrast, parameter-efficient fine-tuning (PEFT) restricts updates to a small subset of parameters while freezing the rest, including adapters and prompt-based techniques. For instance, LORA [19] and its variants restrict Δ to a low-rank correction using matrix factorization.

After fine-tuning, these methods apply the learned modification to every input, *i.e.*, they are input-agnostic. Although the resulting functional change can still vary with the input through the model’s activations, the update itself has no mechanism for selectively turning off on inputs where the pre-trained behavior should be preserved. As a result, both fine-tuning-domain inputs, where modification is beneficial, and pre-training-domain inputs, where the original behavior should be preserved, are affected equally. To study this source of forgetting, we analyze a minimal linear regression model in which both pre-training and fine-tuning data remain available throughout training. We show that even in this favorable scenario, any fixed additive update of the form (1) must compromise between fitting the fine-tuning data and preserving the pre-trained mapping.

A minimal model of adaptation and retention. Let p_{ft} and p_{pt} denote the fine-tuning and pre-training data distributions, and let $\mathbf{W}_0 \in \mathbb{R}^{d_y \times d_x}$ denote the pre-trained model. Each training pair (\mathbf{x}, \mathbf{y}) is sampled from the symmetric mixture of the two populations as follows:

$$\mathbf{x} \sim \begin{cases} p_{\text{ft}} & \text{w.p. } 1/2, \\ p_{\text{pt}} & \text{w.p. } 1/2, \end{cases} \quad \mathbf{y} = \begin{cases} (\mathbf{W}_0 + \mathbf{M})\mathbf{x} & \text{when } \mathbf{x} \sim p_{\text{ft}}, \\ \mathbf{W}_0\mathbf{x} & \text{when } \mathbf{x} \sim p_{\text{pt}}, \end{cases} \quad (2)$$

where $\mathbf{M} \in \mathbb{R}^{d_y \times d_x}$ is an arbitrary task-specific matrix. This setting is strictly easier than sequential fine-tuning since both populations are available throughout training. Adaptation is therefore required on p_{ft} , while the original mapping should be preserved on p_{pt} , leading to the following objective:

$$\mathcal{L}(\Delta) = \frac{1}{2} \mathbb{E}_{p_{\text{ft}}} \left[\|\Delta \mathbf{x}\|_2^2 \right] + \frac{1}{2} \mathbb{E}_{p_{\text{pt}}} \left[\|\Delta \mathbf{x}\|_2^2 \right]. \quad (3)$$

Let $\Sigma_{\mathbf{x}\mathbf{x}}^{\text{ft}}$ and $\Sigma_{\mathbf{x}\mathbf{x}}^{\text{pt}}$ be the second-moment matrices under the distributions p_{ft} and p_{pt} . To expose the conflict in its simplest form, suppose $\Sigma_{\mathbf{x}\mathbf{x}}^{\text{ft}} = \Sigma_{\mathbf{x}\mathbf{x}}^{\text{pt}} =: \Sigma_{\mathbf{x}\mathbf{x}}$. Thus, the unconstrained optimum is

$$\Delta^* = \frac{1}{2} \mathbf{M}, \quad \mathcal{L}(\Delta^*) = \frac{1}{4} \text{Tr}(\mathbf{M} \Sigma_{\mathbf{x}\mathbf{x}} \mathbf{M}^\top). \quad (4)$$

In this linear setting, full FT corresponds to optimizing an unconstrained fixed matrix Δ , while LORA further restricts Δ to a low-rank factorization. Imposing additional constraints on Δ , such as a low-rank factorization, can only increase the loss, so $\mathcal{L}(\Delta^*)$ is a lower bound for any fixed-update method. However, even this best fixed update achieves neither full adaptation on p_{ft} nor zero forgetting on p_{pt} : it applies only half of the desired correction on fine-tuning inputs and a nonzero half-correction on pre-training inputs. This reflects a structural conflict arising from using the same fixed matrix across both populations. Figure 1 confirms this empirically: both LORA and full FT incur non-negligible MSE on each population, illustrating the tradeoff.

This limitation can be mitigated by allowing the correction to depend on the input. In this regression model, the optimal input-dependent correction takes the form (see derivation in Appendix I):

$$f^*(\mathbf{x}) = \pi_{\text{ft}}(\mathbf{x}) \mathbf{M} \mathbf{x}, \quad \pi_{\text{ft}}(\mathbf{x}) = \frac{p_{\text{ft}}(\mathbf{x})}{p_{\text{ft}}(\mathbf{x}) + p_{\text{pt}}(\mathbf{x})} \in [0, 1]. \quad (5)$$

Here $\pi_{\text{ft}}(\mathbf{x})$ is the posterior probability that an input with value \mathbf{x} was drawn from the fine-tuning population under the symmetric mixture. Thus, the update is large on inputs that are likely under the fine-tuning distribution and small on inputs that are likely under the pre-training distribution. This correction achieves the minimum possible squared-error loss for the problem; in the special case where the two distributions have disjoint support, $\pi_{\text{ft}}(\mathbf{x})$ is an indicator and the loss becomes zero.

When the two populations are multivariate Gaussian with the same covariance Σ and different means $\mu_{\text{ft}} \neq \mu_{\text{pt}}$, the log density ratio is affine in \mathbf{x} , and the optimal correction thus admits the closed form

$$f^*(\mathbf{x}) = \sigma(\mathbf{w}_g^\top \mathbf{x} + b_g) \mathbf{M} \mathbf{x}, \quad (6)$$

where $\sigma(x) := 1/(1 + e^{-x}) \in [0, 1]$ for $x \in \mathbb{R}$ is the sigmoid function, and

$$\mathbf{w}_g := \Sigma^{-1}(\mu_{\text{ft}} - \mu_{\text{pt}}) \in \mathbb{R}^d, \quad b_g := \frac{1}{2} (\mu_{\text{pt}}^\top \Sigma^{-1} \mu_{\text{pt}} - \mu_{\text{ft}}^\top \Sigma^{-1} \mu_{\text{ft}}) \in \mathbb{R}. \quad (7)$$

The full derivations can be found in Appendix I.

From (6), we see that the optimal correction in this case is a *sigmoid of an affine transformation of \mathbf{x}* , applied to the fine-tuning update $\mathbf{M} \mathbf{x}$. This motivates the introduction of an input-dependent sigmoid gate $\sigma(\mathbf{w}_g^\top \mathbf{x} + b_g)$ for LLM fine-tuning, where \mathbf{w}_g and b_g are learnable parameters. This gate acts as a soft switch, activating (values near 1) for fine-tuning inputs and suppressing (values near 0) for pre-training inputs. To further gain expressiveness, we extend this scalar gate to a vector-valued one, assigning a separate gate to each rank-one component of the modification. This yields a gating vector $\sigma(\mathbf{W}_g \mathbf{x} + \mathbf{b}_g) \in [0, 1]^r$, which we formalize in the next section.

3 DISeL: Dynamic Input-Sensitive LORA

In Sec. 2, we saw that applying a fixed correction Δ for all inputs induces a compromise between task adaptation and preserving the pre-trained mapping, whereas the Bayes-optimal predictor avoids this by conditioning the correction on the input. Thus, let us consider a general adapter of the form

$$\mathbf{y} = \mathbf{W}_0 \mathbf{x} + f(\mathbf{x}; \theta), \quad (8)$$

where $f: \mathbb{R}^{d_x} \rightarrow \mathbb{R}^{d_y}$ is a trainable mapping. The desired behavior for f is to provide the necessary adaptation on inputs from p_{ft} , while vanishing on inputs from p_{pt} . Meanwhile, the method should remain memory and computationally efficient to ensure practical applicability.

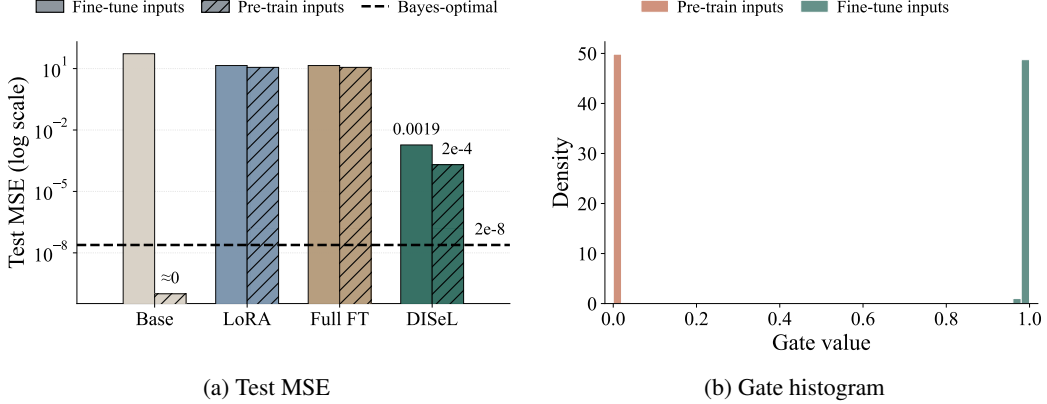


Figure 1: **Selective adaptation toy example.** We minimize the loss in (3) on inputs drawn from a symmetric mixture of two Gaussian populations (see Appendix I for details). Panel (a) shows the test MSE on fine-tuning and pre-training inputs. Here, LoRA and full FT reach the fixed-correction tradeoff, whereas DiSeL achieves much lower error on both domains, approaching the Bayes-optimal error floor (dashed line). Panel (b) plots the activation of the learned gates in DiSeL. We see that the activations concentrate near 1 for fine-tuning inputs and near 0 for pre-training inputs, confirming that the update is activated only when adaptation is needed.

Method. To this end, we build our approach based on LoRA, a widely adopted PEFT method, which freezes \mathbf{W}_0 and learns a low-rank correction as a product $\mathbf{A}\mathbf{B}\mathbf{x}$ with $\mathbf{A} \in \mathbb{R}^{d_y \times r}$ and $\mathbf{B} \in \mathbb{R}^{r \times d_x}$. The key idea behind DiSeL is to multiply each rank-one component by an input-dependent scalar gate $g_i(\mathbf{x}) \in [0, 1]$. Collecting these into a gate vector $g(\mathbf{x}) = (g_1(\mathbf{x}), \dots, g_r(\mathbf{x}))^\top$ and a diagonal matrix $\mathbf{G}(\mathbf{x}) = \text{diag}(g(\mathbf{x}))$, the DiSeL adaptation is defined as

$$f(\mathbf{x}; \theta) = \mathbf{A}\mathbf{G}(\mathbf{x})\mathbf{B}\mathbf{x} = \sum_{i=1}^r g_i(\mathbf{x})\mathbf{a}_i\mathbf{b}_i^\top \mathbf{x}, \quad (\text{DiSeL})$$

where \mathbf{a}_i and \mathbf{b}_i^\top are \mathbf{A} 's columns and \mathbf{B} 's rows, respectively. The gate vector is parameterized as

$$g(\mathbf{x}) = \sigma(\mathbf{W}_g\mathbf{x} + \mathbf{b}_g) \in [0, 1]^r, \quad (9)$$

with $\mathbf{W}_g \in \mathbb{R}^{r \times d_x}$, $\mathbf{b}_g \in \mathbb{R}^r$, and $\sigma(z) = 1/(1 + e^{-z})$ applied element-wise. We use a sigmoid rather than a softmax so that gates act as independent soft switches, allowing multiple rank-one components to be active at the same time, or all inactive simultaneously, for the same input.

Memory and inference overhead. DiSeL introduces additional $rd_x + r$ parameters per adapted block, with a total of $rd_y + 2rd_x + r$ trainable parameters, comparable to $rd_y + rd_x$ of LoRA. The gate computation requires $\mathcal{O}(d_x r)$ arithmetic operations, negligible relative to the cost of the linear projection $\mathbf{W}_0\mathbf{x}$. Overall, both the memory and computational overhead are comparable to LoRA.

Initialization and approximation of the Bayes predictor. During fine-tuning, we typically observe only data from p_{ft} , whereas the Bayes-optimal predictor relies on both populations to identify which inputs require adaptation. Without access to p_{pt} , we cannot directly enforce $f(\mathbf{x}; \theta) \approx \mathbf{0}$ on pre-training-domain inputs; instead, we encode this as the *default* behavior at initialization. Specifically, we initialize \mathbf{b}_g to a small negative value, such that $\sigma(\mathbf{b}_g)$ is approximately zero, and initialize \mathbf{W}_g using a standard scheme, e.g., He et al. [17]. Combined with the standard LoRA initialization, this makes DiSeL start equal to the pre-trained model on all inputs. During training, gates are activated only when this reduces the FT loss, yielding an approximation to the Bayes-optimal input-dependent correction. The initialization of \mathbf{b}_g is a hyperparameter that may depend on the task and dataset; in our LLAMA and MISTRAL experiments, we set $\mathbf{b}_g = -3 \cdot \mathbf{1}$, where $\sigma(-3) \approx 0.05$.

Gates learning vs. A, B fine-tuning. The factors \mathbf{A} and \mathbf{B} play the same role as in standard LoRA: they parameterize the adaptation itself and thus are tuned with a small learning rate. In contrast, the gate parameters $(\mathbf{W}_g, \mathbf{b}_g)$ learn a new and different task: to distinguish fine-tuning inputs from the rest of the input space, so that the update $\mathbf{A}\mathbf{B}\mathbf{x}$ is applied selectively. This is more akin to representation learning during pre-training than to a small refinement of an existing linear map.

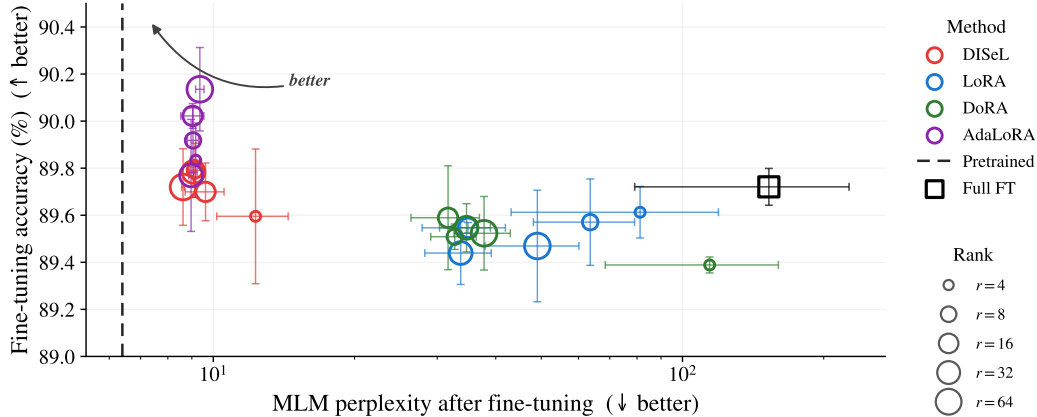


Figure 2: **ROBERTa on GLUE**. We fine-tune ROBERTa-base on five GLUE tasks: MNLI, SST-2, QNLI, CoLA, and MRPC, using various methods and ranks. The vertical axis measures the average test accuracy for the corresponding tasks, while the horizontal axis indicates the average masked-LM perplexity, evaluated on BOOKCORPUSOPEN, CC-NEWS, and WIKITEXT-2. Each point represents a method-rank pair averaged across three seeds, with error bars indicating the standard deviation. The dashed line marks the pre-trained baseline. Here, DISeL and ADALORA remain close to this baseline while matching the FT accuracy of full FT, whereas the other methods forget much more.

Accordingly, we treat (\mathbf{A}, \mathbf{B}) and $(\mathbf{W}_g, \mathbf{b}_g)$ as two distinct optimization problems and assign them *separate learning rates*, with the gate learning rate substantially larger. In our LLAMA and MISTRAL experiments, we use a learning rate $5\times$ larger for the gate parameters than for \mathbf{A} and \mathbf{B} .

4 Experiments

In this section, we evaluate the downstream performance of DISeL in two settings: (i) fine-tuning ROBERTa-base [29] on the GLUE benchmark [47] (Section 4.1), and (ii) instruction tuning of LLAMA 2-7B [46] and MISTRAL-7B [21] on mathematical reasoning and code generation tasks (Section 4.2). For each setting, we report two quantities: fine-tuning task performance and forgetting on benchmarks outside the fine-tuning domain. We compare DISeL against full fine-tuning and three widely used PEFT baselines: LORA [19], DORA [28], and ADALORA [62].

4.1 ROBERTa on GLUE

Setup. We fine-tune ROBERTa-base on five GLUE tasks: MNLI, SST-2, QNLI, CoLA, and MRPC. For each task, we consider ranks $r \in \{4, 8, 16, 32, 64\}$. Fine-tuning performance is measured as the average test accuracy across tasks. The forgetting is quantified via masked language modeling (MLM) perplexity of the fine-tuned model on BOOKCORPUSOPEN [1], CC-NEWS [32], and WIKITEXT-2 [35], where the pre-trained model achieves an averaged perplexity of ≈ 6.4 on these datasets. Each configuration (method, task, rank) is evaluated over three random seeds, and we report the mean \pm standard deviation. Full details are provided in Appendix II.

Figure 2 plots the FT accuracy against retention. While most methods achieve comparable FT accuracy, they differ substantially in retention performance. Full fine-tuning attains high accuracy but deviates most strongly from the pre-trained baseline, yielding a mean perplexity of roughly 150. Fixed-rank adapters such as LORA and DORA mitigate this effect at the cost of slightly reduced FT accuracy, but still incur substantial forgetting, with perplexity ranging from 30 to 100. By contrast, DISeL and ADALORA remain close to the pre-trained baseline, with perplexity around 9, while matching or surpassing the accuracy of full fine-tuning. DISeL thus achieves a similarly favorable tradeoff between accuracy and forgetting as pruning-based ADALORA, without requiring a pruning schedule. Although ADALORA performs competitively on this benchmark, the next section shows that its FT accuracy degrades at larger scales and on more challenging tasks, such as mathematical reasoning and code generation.

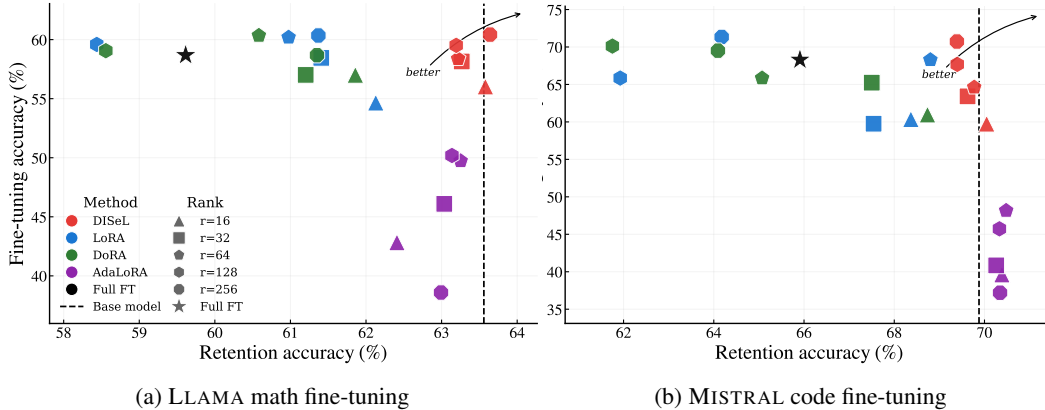


Figure 3: **LLAMA and MISTRAL instruction fine-tuning.** We fine-tune LLAMA and MISTRAL on math and code instructions, respectively, with various methods using different ranks. Panel (a) shows the results for LLAMA, whereas Panel (b) depicts them for MISTRAL. Here, the vertical axis shows test accuracy for the corresponding fine-tuning task, and the horizontal axis shows the average accuracy across several pre-training tasks. The dashed vertical line marks the accuracy of the pre-trained model. This experiment shows that DISeL achieves competitive fine-tuning accuracy without compromising performance on the pre-training tasks.

4.2 LLAMA and MISTRAL on mathematical reasoning and code generation

Setup. We extend our evaluation to large-scale instruction fine-tuning tasks. Specifically, we fine-tune LLAMA 2-7B on METAMATH [59] for math reasoning, and MISTRAL-7B on MAGICODER [55] for code generation. We evaluate FT performance on GSM8K [9] for math, and HUMANEVAL [5] for code. For each model, we use ranks $r \in \{16, 32, 64, 128, 256\}$. To measure forgetting, we evaluate retention on 14 out-of-domain benchmarks, spanning commonsense reasoning, world knowledge, reading comprehension, and medical question answering, and report their unweighted mean accuracy. Appendix III lists the full benchmark suite and per-method hyperparameters.

Figure 3 visualizes the tradeoff between fine-tuning and retention. Here, DISeL achieves strong task accuracy while maintaining retention close to the base model. On LLAMA, it reaches around 60% FT accuracy with retention near 63.3%, only slightly below the base model. On MISTRAL, our approach exceeds 70% FT accuracy while maintaining retention within a fraction of a percentage point of the base model ($\approx 70\%$). The occasional improvement over base-model retention suggests that fine-tuning can also improve the general reasoning abilities probed by some retention benchmarks.

In contrast, full FT attains reasonable task accuracy but incurs substantial forgetting, shifting far left of the base-model retention line and failing to dominate the adapter methods. Its relatively small forgetting compared with the worst adapter runs is partly explained by the smaller learning rate used for fine-tuning. Among the three other PEFT methods, ADALORA matches DISeL in retention, as in the ROBERTa experiments, but its FT accuracy drops to roughly 40–50% on both models. LORA and DORA perform competitively at low ranks, but their retention deteriorates as rank increases, losing 4–8% at the largest ranks. By comparison, DISeL achieves consistent performance across ranks, models, and datasets, preserving both task performance and pre-training capability.

This robustness is practically useful beyond the final accuracy–retention tradeoff itself. Recent work has shown that LORA’s performance can be highly sensitive to learning rate, rank, initialization, and scaling choices, often requiring careful tuning to achieve strong performance [6]. In contrast, the gating mechanism of DISeL provides implicit regularization by limiting the effective modification of inactive or weakly activated components, thereby stabilizing training at larger or suboptimal adapter learning rates. Moreover, the separate learning rate for the gates also provides a direct control knob for the plasticity–retention tradeoff: larger gate learning rates encourage more gates to open and favor adaptation to the new task, whereas smaller gate learning rates keep more directions closed and favor retention of pre-training knowledge.

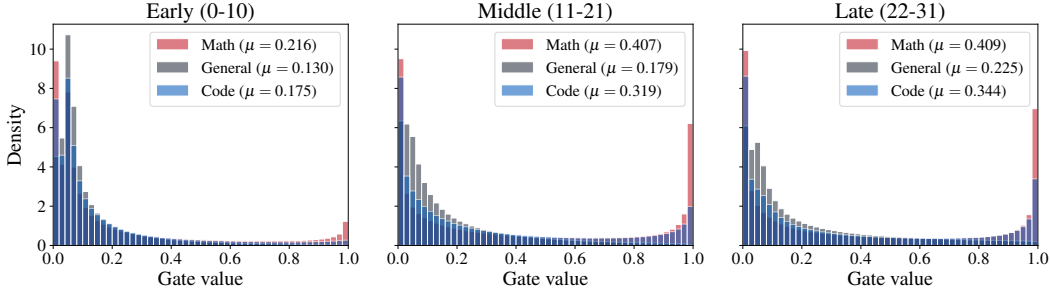


Figure 4: **Gate activation histograms across domains.** We analyze gate activations of a rank-32 LLAMA math adapter on held-out samples from math, general text, and code. Each panel corresponds to a layer-depth band: early, middle, or late layers. Here, the gates are substantially more open for math inputs, the fine-tuning domain, than for general text from the pre-training distribution. The largest differences appear in the middle and later layers. This demonstrates that DISeL selectively applies adaptation on inputs from the fine-tuned distribution.

5 Interpretability of DISeL

Setup. The main idea behind DISeL is that its gates are *input-dependent*. Specifically, the adapter correction should be active for inputs from the fine-tuning task, and suppressed for others. Here, we examine whether this behavior indeed emerges in trained models by analyzing the gate activations during inference. For this, we use held-out sequences from three domains: math, general text, and code. Math samples are drawn from the GSM8K test set, formatted with the same instruction–response template used during LLAMA fine-tuning. General-text samples are raw passages from the WIKITEXT-2 test set. Code samples are taken from HUMANEVAL test problems. For math and code, we consider gates on the response tokens, whereas for raw general-text, we measure gates over all tokens. For each sample, we record the post-sigmoid values at each adapted layer during the forward pass. We then aggregate the gate values, dividing the layers into three depth groups (early, mid, late), and create a normalized histogram for each group. Throughout this section, we present results for the rank-32 LLAMA 2-7B adapter fine-tuned for mathematical reasoning from Section 4.2. Additional results for LLAMA and MISTRAL are given in Appendix V.

Domain analysis. Figure 4 shows gate activations across different input domains. In early layers, the gates are nearly closed across all domains, suggesting that adaptation in these layers might not be needed. Yet, in the middle and late layers, there is a clear separation: math samples have substantially larger gate values than general text, while code lies between the two. This ordering makes sense in this setup: math is the fine-tuning domain, general text is outside that domain, and code shares some structured-symbolic and logical reasoning with math. Overall, the gates are not static; they open more to inputs from the fine-tuning domain than to those from the pre-trained domain.

Module analysis. In Figure 5, we fix the input domain to held-out math examples and compare selected adapted layer types: the attention module (v_{proj}), the MLP up projection (up_{proj}), and the MLP down projection ($\text{down}_{\text{proj}}$). Here we see that gate activation is highly non-uniform across different module types. The MLP up projection has the largest gate values, especially in middle and late layers; the down projection shows a weaker version of the same trend; and the value projection remains comparatively closed. This suggests that the learned gates provide a useful diagnostic for where task-specific adapter capacity is used, and may help improve the design of future modules. Taken together, Figures 4 and 5 demonstrate that DISeL learns a conditional routing pattern: gate usage varies across input domains and concentrates in specific parts of the network rather than being distributed uniformly across all ranks, layers, and modules.

6 Retention over time

The tradeoff plots in Section 4 report retention at the best target-task checkpoint, but do not reveal how retention *evolves* during training. A method may end close to the base model while passing through degraded intermediate states, or it may lose capability steadily from the first few optimization steps. To distinguish these regimes, we track retention at every saved checkpoint of the LLAMA 2-7B,

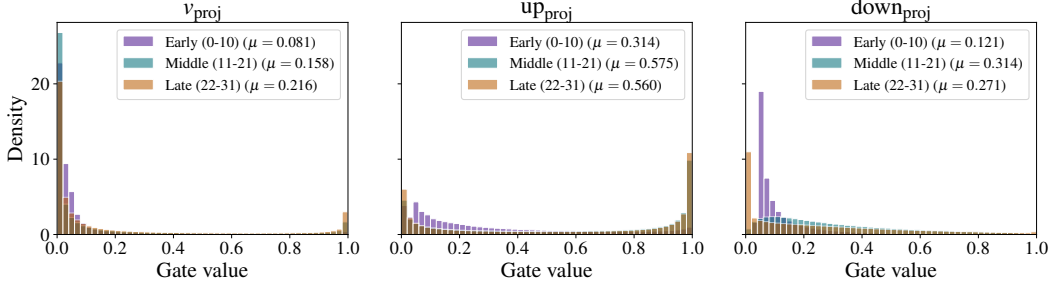


Figure 5: **Layer-wise gate usage within key modules.** We processed held-out math samples with LLAMA using a rank-32 DISeL adapter and measured the output distributions of each module’s gates. This figure presents these distributions for the attention value projection (v_{proj}), the MLP up projection (up_{proj}), and the MLP down projection ($down_{\text{proj}}$). Each panel shows normalized histograms for early, middle, and late layers. In this example, the gates are most open in the MLP up projection, especially in the middle and late layers, while the value and down projections exhibit more moderate activation. This demonstrates that DISeL learns not only when to activate adapter components, but also where in the model those components are most useful.

for ranks $r \in \{16, 32, 64, 128, 256\}$. As before, retention is measured as the mean accuracy over the 14-benchmark suite from Section 4.2. Additional results are provided in Appendix IV.

Figure 6 shows the resulting trajectories for DISeL (left) and LORA (right). For LORA, retention degrades progressively with rank: at $r=16$, it remains within about one percentage point of the base model, but at higher ranks it exhibits a clear downward drift, falling roughly a 5% at the largest ranks. This degradation is persistent rather than transient; once lost, performance does not recover within the training horizon. In contrast, DISeL maintains near-flat retention curves across all ranks, with deviations remaining within about half a percentage point of the base model from the first checkpoint to the last. This stability can be attributed to the fact that input-dependent gates keep the correction largely inactive on inputs outside the fine-tuning distribution, preventing increased capacity from inducing additional drift. As a result, DISeL effectively decouples adapter rank from forgetting, enabling the use of larger ranks without sacrificing retention.

Finally, we observe that forgetting could also depend on the optimization setting. For LORA, the $r=128$ run exhibits more forgetting than $r=256$, as the latter required a smaller learning rate (10^{-4}) for stability, whereas the former uses a twice larger step size. A similar effect appears in Figure 3, where Full FT does not incur the largest forgetting, partly due to its smaller learning rate used (10^{-5}).

7 Related work

We discuss three lines of work most related to DISeL: parameter-efficient low-rank fine-tuning, input-conditional and mixture-style adapters, and continual learning of pre-trained models.

Parameter-efficient and low-rank fine-tuning. LORA [19] approximates the FT update using a fixed low-rank correction $\Delta = \mathbf{A}\mathbf{B}$ added to a frozen pre-trained weight, and has become the dominant approach to parameter-efficient adaptation. A large body of follow-up work refines the *parameterization* of Δ : ADALORA [62] adapts the rank budget across layers, DORA [28] decouples magnitude from direction, PiSSA [34] initializes \mathbf{A}, \mathbf{B} from the principal singular subspace of \mathbf{W} , LORA-GA [50] chooses the initialization such that the first gradient step approximates full FT, VERA [25] freezes shared random \mathbf{A}, \mathbf{B} and learns only a diagonal scaling between them, structurally close to the $\mathbf{G}(\mathbf{x})$ in DISeL but fixed across inputs, and AURORA [14] introduces a nonlinear coupling between the factors. Other variants modify optimization dynamics: LORA+ [16] uses asymmetric learning rates for \mathbf{A} and \mathbf{B} , LORAM [22] optimizes the low-rank adapter on Riemannian manifolds, and QLORA [10] combines low-rank adaptation with weight quantization. Despite their differences, these methods produce a single correction matrix that is uniformly applied to every input during inference. DISeL preserves the low-rank parameterization and matches the computational efficiency of LORA, while making the correction input-dependent through lightweight gates. This selective adaptation mechanism directly addresses the structural conflict identified in Section 2.

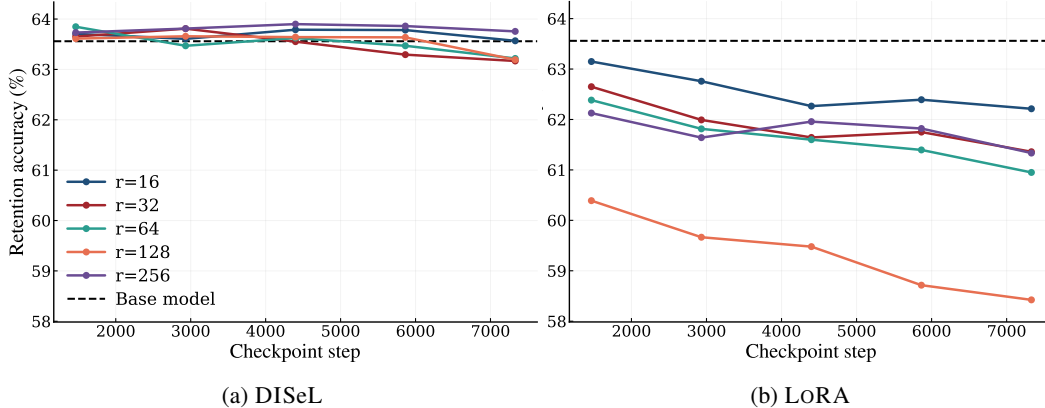


Figure 6: **Retention vs. training step.** We evaluate the retention performance during fine-tuning from the experiment in Sec. 4.2. Here we present the results for LLAMA 2- 7B model fine-tuned on METAMATHQA using LORA and DISeL with various ranks. Panel (a) shows the result for DISeL, while Panel (b) plots them for LORA. We see that DISeL maintains near-zero retention drop at every rank, including the largest, whereas LORA’s retention deteriorates with both rank and training time.

Input-conditional and mixture-of-LORA approaches. A separate line of work introduces input- or task-conditional adaptation by combining *multiple* LORA modules. MOLE [58] routes between several LORA adapters via a learned gating network, in the spirit of mixture-of-experts. LORAHUB [20] composes pre-trained task-specific LORA modules into a single weighted combination selected for each downstream task. These approaches operate at the coarse-grained level of entire adapters, and scale both the parameter count and the routing cost with the number of modules. The closest architectural prior is GATED LORA [15], which treats each rank-one component as a mini-expert, and selects the active components based on the input. Specifically, it uses a ReLU activation function on the same down-projection features used to compute the LORA update, thereby avoiding a separate router. Its primary goal is to improve parameter utilization and reduce inter-task interference, especially in multi-task fine-tuning. Similar to GATED LORA, DISeL also gates rank-one components inside a single adapter. However, DISeL uses separate learnable sigmoid gates initialized near zero so that the default behavior matches the pre-trained model. More importantly, our objective is fundamentally different: rather than improving multi-task routing, DISeL is designed to preserve pre-trained behavior on inputs outside the fine-tuning distribution.

Continual learning. Continual learning methods adapt a pre-trained model to a sequence of tasks while preserving previously acquired knowledge. GAINLORA [27] introduces a separate LORA branch for each new task and learns gates that limit interference between branches. Related prompt-based methods, including DUALPROMPT [52], S-PROMPTS [51], HiDE-PROMPT [48], and mixture-style prefix tuning [26], route inputs among task- or domain-specific prompts, while RANPAC [33] avoids backbone updates entirely by learning class prototypes after a fixed random projection. These methods address forgetting across a sequence of tasks and typically operate at the level of entire adapters, prompts, or task-specific classifiers. DISeL instead targets the retention-adaptation tradeoff within a *single* fine-tuning task, using continuous input-dependent gating over rank-one components inside a single LORA adapter, without requiring task identities or routing labels.

8 Conclusion

We introduced DISeL, an FT method that addresses the input-agnostic nature of standard adapter updates. While LORA learns a fixed correction that is applied to every input, DISeL makes this correction input-dependent by placing lightweight gates on individual rank-one components. This design is motivated by the tension identified in our linear analysis: a fixed update must compromise between adapting to fine-tuning-domain inputs and preserving the pre-trained mapping elsewhere.

Across ROBERTa on GLUE and instruction tuning of LLAMA and MISTRAL models on mathematical reasoning and code generation, DISeL achieves a favorable tradeoff between FT accuracy and retention. It keeps retention close to the base model while maintaining competitive task performance.

The learned gates further strengthen the interpretability angle of DISeL: they reveal when the adapter is activated, which inputs induce stronger adaptation, and where in the network task-specific capacity is concentrated. This makes DISeL useful not only as a retention-preserving FT method, but also as a diagnostic tool for understanding and potentially controlling adaptation.

Limitations and future work. DISeL does not guarantee preservation of all pre-trained capabilities, and its behavior depends on choices such as gate initialization, gate learning rate, and the adapted modules. Moreover, while effective in single-task FT, it remains unclear how best to extend input-dependent adaptation to multi-task or continual learning, or how to merge the learned adapter into the base weights for sustainable deployment. Future work could combine DISeL with explicit retention objectives, use gate statistics for adaptive rank selection, and evaluate the method in broader settings such as alignment, multilingual transfer, long-context adaptation, and continual learning.

Acknowledgment

This work was supported by the Helmholtz Association’s Initiative and Networking Fund on the HAICORE@FZJ partition. Part of this work was carried out while S.U. Stich was visiting the Simons Institute for the Theory of Computing. We also gratefully acknowledge funding from the European Research Council (ERC) under the Horizon Europe Framework Programme (HORIZON) for proposal number 101170430 CollectiveMinds. Views and opinions expressed are however those of the authors only and do not necessarily reflect those of the European Union or the European Research Council. Neither the European Union nor the granting authority can be held responsible for them.

References

- [1] Jack Bandy and Nicholas Vincent. Addressing "documentation debt" in machine learning research: A retrospective datasheet for bookcorpus. *arXiv preprint arXiv:2105.05241*, 2021.
- [2] Dan Biderman, Jacob Portes, Jose Javier Gonzalez Ortiz, Mansheej Paul, Philip Greengard, Connor Jennings, Daniel King, Sam Havens, Vitaliy Chiley, Jonathan Frankle, et al. LoRA learns less and forgets less. *Transactions on Machine Learning Research*, 2024.
- [3] Yonatan Bisk, Rowan Zellers, Ronan Le Bras, Jianfeng Gao, and Yejin Choi. PIQA: Reasoning about physical commonsense in natural language. In *Thirty-Fourth AAAI Conference on Artificial Intelligence*, 2020.
- [4] Eric L Buehler and Markus J Buehler. X-LoRA: Mixture of low-rank adapter experts, a flexible framework for large language models with applications in protein mechanics and molecular design. *APL Machine Learning*, 2(2), 2024.
- [5] Mark Chen, Jerry Tworek, Heewoo Jun, Qiming Yuan, Henrique Ponde De Oliveira Pinto, Jared Kaplan, Harri Edwards, Yuri Burda, Nicholas Joseph, Greg Brockman, et al. Evaluating large language models trained on code. *arXiv preprint arXiv:2107.03374*, 2021.
- [6] Nan Chen, Soledad Villar, and Soufiane Hayou. Learning rate scaling across LoRA ranks and transfer to full finetuning. *arXiv preprint arXiv:2602.06204*, 2026.
- [7] Christopher Clark, Kenton Lee, Ming-Wei Chang, Tom Kwiatkowski, Michael Collins, and Kristina Toutanova. BoolQ: Exploring the surprising difficulty of natural yes/no questions. In *Proceedings of the 2019 Conference of the North American Chapter of the Association for Computational Linguistics: Human Language Technologies (Volume 1: Long and Short Papers)*. Association for Computational Linguistics, 2019.
- [8] Peter Clark, Isaac Cowhey, Oren Etzioni, Tushar Khot, Ashish Sabharwal, Carissa Schoenick, and Oyvind Tafjord. Think you have solved question answering? Try ARC, the AI2 reasoning challenge. *arXiv:1803.05457*, 2018.
- [9] Karl Cobbe, Vineet Kosaraju, Mohammad Bavarian, Mark Chen, Heewoo Jun, Lukasz Kaiser, Matthias Plappert, Jerry Tworek, Jacob Hilton, Reiichiro Nakano, et al. Training verifiers to solve math word problems. *arXiv preprint arXiv:2110.14168*, 2021.

- [10] Tim Dettmers, Artidoro Pagnoni, Ari Holtzman, and Luke Zettlemoyer. QLoRA: Efficient finetuning of quantized LLMs. In *Advances in Neural Information Processing Systems*. Curran Associates, Inc., 2023.
- [11] Jacob Devlin, Ming-Wei Chang, Kenton Lee, and Kristina Toutanova. BERT: Pre-training of deep bidirectional transformers for language understanding. In *Proceedings of the 2019 Conference of the North American Chapter of the Association for Computational Linguistics: Human Language Technologies (Volume 1: Long and Short Papers)*. Association for Computational Linguistics, 2019.
- [12] William B Dolan and Chris Brockett. Automatically constructing a corpus of sentential paraphrases. In *Proceedings of the Third International Workshop on Paraphrasing (IWP2005)*, 2005.
- [13] Guanting Dong, Hongyi Yuan, Keming Lu, Chengpeng Li, Mingfeng Xue, Dayiheng Liu, Wei Wang, Zheng Yuan, Chang Zhou, and Jingren Zhou. How abilities in large language models are affected by supervised fine-tuning data composition. In *Proceedings of the 62nd Annual Meeting of the Association for Computational Linguistics (Volume 1: Long Papers)*, pages 177–198, 2024.
- [14] Haonan Dong, Wenhao Zhu, Guojie Song, and Liang Wang. AuroRA: Breaking low-rank bottleneck of LoRA with nonlinear mapping. In *Advances in Neural Information Processing Systems*. Curran Associates, Inc., 2025.
- [15] SooHwan Eom, Hee Suk Yoon, Eunseop Yoon, Mark A Hasegawa-Johnson, and Chang D Yoon. Gated LoRA: Dual-purpose projections for parameter-efficient mini-expert fine-tuning. In *Submitted to International Conference on Learning Representations*, 2025.
- [16] Soufiane Hayou, Nikhil Ghosh, and Bin Yu. LoRA+: Efficient low rank adaptation of large models. In *Proceedings of the 41st International Conference on Machine Learning*. PMLR, 2024.
- [17] Kaiming He, Xiangyu Zhang, Shaoqing Ren, and Jian Sun. Delving deep into rectifiers: Surpassing human-level performance on ImageNet classification. In *Proceedings of the IEEE International Conference on Computer Vision*, pages 1026–1034, 2015.
- [18] Dan Hendrycks, Collin Burns, Steven Basart, Andy Zou, Mantas Mazeika, Dawn Song, and Jacob Steinhardt. Measuring massive multitask language understanding. In *The Ninth International Conference on Learning Representations*, 2021.
- [19] Edward J Hu, Yelong Shen, Phillip Wallis, Zeyuan Allen-Zhu, Yuanzhi Li, Shean Wang, Lu Wang, and Weizhu Chen. LoRA: Low-rank adaptation of large language models. In *The Tenth International Conference on Learning Representations*, 2022.
- [20] Chengsong Huang, Qian Liu, Bill Yuchen Lin, Tianyu Pang, Chao Du, and Min Lin. LoraHub: Efficient cross-task generalization via dynamic LoRA composition. In *First Conference on Language Modeling*, 2024.
- [21] Albert Q. Jiang, Alexandre Sablayrolles, Arthur Mensch, Chris Bamford, Devendra Singh Chaplot, Diego de las Casas, Florian Bressand, Gianna Lengyel, Guillaume Lample, Lucile Saulnier, L lio Renard Lavaud, Marie-Anne Lachaux, Pierre Stock, Teven Le Scao, Thibaut Lavril, Thomas Wang, Timoth e Lacroix, and William El Sayed. Mistral 7B, 2023.
- [22] Xiaowen Jiang, Xun Wang, and Sebastian U. Stich. LoRAM: Low-rank adaptation of large language models on manifold. In *Sparsity in LLMs (SLLM): Deep Dive into Mixture of Experts, Quantization, Hardware, and Inference*, 2025.
- [23] Di Jin, Eileen Pan, Nassim Oufattole, Wei-Hung Weng, Hanyi Fang, and Peter Szolovits. What disease does this patient have? A large-scale open domain question answering dataset from medical exams. *arXiv preprint arXiv:2009.13081*, 2020.
- [24] Mandar Joshi, Eunsol Choi, Daniel S Weld, and Luke Zettlemoyer. TriviaQA: A large scale distantly supervised challenge dataset for reading comprehension. In *Proceedings of the 55th Annual Meeting of the Association for Computational Linguistics*, pages 1601–1611, 2017.

- [25] Dawid Kopiczko, Tijmen Blankevoort, and Yuki Asano. VeRA: Vector-based random matrix adaptation. In *The Twelfth International Conference on Learning Representations*, 2024.
- [26] Minh Le, An Nguyen, Huy Nguyen, Trang Nguyen, Trang Pham, Linh Van Ngo, and Nhat Ho. Mixture of experts meets prompt-based continual learning. In *Advances in Neural Information Processing Systems*. Curran Associates, Inc., 2024.
- [27] Yan-Shuo Liang, Jia-Rui Chen, and Wu-Jun Li. Gated integration of low-rank adaptation for continual learning of large language models. In *Advances in Neural Information Processing Systems*. Curran Associates, Inc., 2025.
- [28] Shih-Yang Liu, Chien-Yi Wang, Hongxu Yin, Pavlo Molchanov, Yu-Chiang Frank Wang, Kwang-Ting Cheng, and Min-Hung Chen. DoRA: Weight-decomposed low-rank adaptation. In *Proceedings of the 41st International Conference on Machine Learning*. PMLR, 2024.
- [29] Yinhan Liu, Myle Ott, Naman Goyal, Jingfei Du, Mandar Joshi, Danqi Chen, Omer Levy, Mike Lewis, Luke Zettlemoyer, and Veselin Stoyanov. RoBERTa: A robustly optimized BERT pretraining approach. *arXiv preprint arXiv:1907.11692*, 2019.
- [30] Yun Luo, Zhen Yang, Fandong Meng, Yafu Li, Jie Zhou, and Yue Zhang. An empirical study of catastrophic forgetting in large language models during continual fine-tuning. *IEEE Transactions on Audio, Speech and Language Processing*, 2025.
- [31] Ziyang Luo, Can Xu, Pu Zhao, Qingfeng Sun, Xiubo Geng, Wenxiang Hu, Chongyang Tao, Jing Ma, Qingwei Lin, and Daxin Jiang. WizardCoder: Empowering code large language models with Evol-Instruct. In *The Twelfth International Conference on Learning Representations*, 2024.
- [32] Joel Mackenzie, Rodger Benham, Matthias Petri, Johanne R Trippas, J Shane Culpepper, and Alistair Moffat. CC-News-En: A large English news corpus. In *Proceedings of the 29th ACM International Conference on Information & Knowledge Management*, 2020.
- [33] Mark D McDonnell, Dong Gong, Amin Parvaneh, Ehsan Abbasnejad, and Anton Van den Hengel. RanPAC: Random projections and pre-trained models for continual learning. In *Advances in Neural Information Processing Systems*. Curran Associates, Inc., 2023.
- [34] Fanxu Meng, Zhaohui Wang, and Muhan Zhang. PiSSA: Principal singular values and singular vectors adaptation of large language models. In *Advances in Neural Information Processing Systems*. Curran Associates, Inc., 2024.
- [35] Stephen Merity, Caiming Xiong, James Bradbury, and Richard Socher. Pointer sentinel mixture models. In *The Fifth International Conference on Learning Representations*, 2017.
- [36] Todor Mihaylov, Peter Clark, Tushar Khot, and Ashish Sabharwal. Can a suit of armor conduct electricity? A new dataset for open book question answering. In *Proceedings of the 2018 Conference on Empirical Methods in Natural Language Processing*, 2018.
- [37] Long Ouyang, Jeffrey Wu, Xu Jiang, Diogo Almeida, Carroll Wainwright, Pamela Mishkin, Chong Zhang, Sandhini Agarwal, Katarina Slama, Alex Ray, et al. Training language models to follow instructions with human feedback. In *Advances in Neural Information Processing Systems*. Curran Associates, Inc., 2022.
- [38] Alec Radford, Jeffrey Wu, Rewon Child, David Luan, Dario Amodei, and Ilya Sutskever. Language models are unsupervised multitask learners, 2019.
- [39] Pranav Rajpurkar, Jian Zhang, Konstantin Lopyrev, and Percy Liang. SQuAD: 100,000+ questions for machine comprehension of text. In *Proceedings of the 2016 Conference on Empirical Methods in Natural Language Processing*, pages 2383–2392, 2016.
- [40] Baptiste Roziere, Jonas Gehring, Fabian Gloeckle, Sten Sootla, Itai Gat, Xiaoqing Ellen Tan, Yossi Adi, Jingyu Liu, Romain Sauvestre, Tal Remez, et al. Code Llama: Open foundation models for code. *arXiv preprint arXiv:2308.12950*, 2023.
- [41] Keisuke Sakaguchi, Ronan Le Bras, Chandra Bhagavatula, and Yejin Choi. WinoGrande: An adversarial winograd schema challenge at scale. *Communications of the ACM*, 2021.

- [42] Reece Shuttlesworth, Jacob Andreas, Antonio Torralba, and Pratyusha Sharma. LoRA vs full fine-tuning: An illusion of equivalence. In *Advances in Neural Information Processing Systems*. Curran Associates, Inc., 2025.
- [43] Richard Socher, Alex Perelygin, Jean Wu, Jason Chuang, Christopher D Manning, Andrew Y Ng, and Christopher Potts. Recursive deep models for semantic compositionality over a sentiment treebank. In *Proceedings of the 2013 Conference on Empirical Methods in Natural Language Processing*, 2013.
- [44] Alon Talmor, Jonathan Herzig, Nicholas Lourie, and Jonathan Berant. CommonsenseQA: A question answering challenge targeting commonsense knowledge. In *Proceedings of the 2019 Conference of the North American Chapter of the Association for Computational Linguistics: Human Language Technologies (Volume 1: Long and Short Papers)*. Association for Computational Linguistics, 2019.
- [45] Chunlin Tian, Zhan Shi, Zhijiang Guo, Li Li, and Chengzhong Xu. HydraLoRA: An asymmetric LoRA architecture for efficient fine-tuning. In *Advances in Neural Information Processing Systems*. Curran Associates, Inc., 2024.
- [46] Hugo Touvron, Louis Martin, Kevin Stone, Peter Albert, Amjad Almahairi, Yasmine Babaei, Nikolay Bashlykov, Soumya Batra, Prajjwal Bhargava, Shruti Bhosale, Dan Bikel, Lukas Blecher, Cristian Canton Ferrer, Moya Chen, Guillem Cucurull, David Esiobu, Jude Fernandes, Jeremy Fu, Wenyin Fu, Brian Fuller, Cynthia Gao, Vedanuj Goswami, Naman Goyal, Anthony Hartshorn, Saghar Hosseini, Rui Hou, Hakan Inan, Marcin Kardas, Viktor Kerkez, Madian Khabsa, Isabel Kloumann, Artem Korenev, Punit Singh Koura, Marie-Anne Lachaux, Thibaut Lavril, Jenya Lee, Diana Liskovich, Yinghai Lu, Yuning Mao, Xavier Martinet, Todor Mihaylov, Pushkar Mishra, Igor Molybog, Yixin Nie, Andrew Poulton, Jeremy Reizenstein, Rashi Rungta, Kalyan Saladi, Alan Schelten, Ruan Silva, Eric Michael Smith, Ranjan Subramanian, Xiaoqing Ellen Tan, Binh Tang, Ross Taylor, Adina Williams, Jian Xiang Kuan, Puxin Xu, Zheng Yan, Iliyan Zarov, Yuchen Zhang, Angela Fan, Melanie Kambadur, Sharan Narang, Aurelien Rodriguez, Robert Stojnic, Sergey Edunov, and Thomas Scialom. Llama 2: Open foundation and fine-tuned chat models, 2023.
- [47] Alex Wang, Amanpreet Singh, Julian Michael, Felix Hill, Omer Levy, and Samuel Bowman. GLUE: A multi-task benchmark and analysis platform for natural language understanding. In *Proceedings of the 2018 EMNLP workshop BlackboxNLP: Analyzing and interpreting neural networks for NLP*, pages 353–355, 2018.
- [48] Liyuan Wang, Jingyi Xie, Xingxing Zhang, Mingyi Huang, Hang Su, and Jun Zhu. Hierarchical decomposition of prompt-based continual learning: Rethinking obscured sub-optimality. In *Advances in Neural Information Processing Systems*. Curran Associates, Inc., 2023.
- [49] Liyuan Wang, Xingxing Zhang, Hang Su, and Jun Zhu. A comprehensive survey of continual learning: Theory, method and application. *IEEE Transactions on Pattern Analysis and Machine Intelligence*, 46(8):5362–5383, 2024.
- [50] Shaowen Wang, Linxi Yu, and Jian Li. LoRA-GA: Low-rank adaptation with gradient approximation. In *Advances in Neural Information Processing Systems*. Curran Associates, Inc., 2024.
- [51] Yabin Wang, Zhiwu Huang, and Xiaopeng Hong. S-prompts learning with pre-trained transformers: An Occam’s razor for domain incremental learning. In *Advances in Neural Information Processing Systems*. Curran Associates, Inc., 2022.
- [52] Zifeng Wang, Zizhao Zhang, Sayna Ebrahimi, Ruoxi Sun, Han Zhang, Chen-Yu Lee, Xiaoqi Ren, Guolong Su, Vincent Perot, Jennifer Dy, et al. DualPrompt: Complementary prompting for rehearsal-free continual learning. In *European Conference on Computer Vision*, pages 631–648. Springer, 2022.
- [53] Alex Warstadt, Amanpreet Singh, and Samuel R Bowman. Neural network acceptability judgments. *Transactions of the Association for Computational Linguistics*, 7:625–641, 2019.

- [54] Jason Wei, Maarten Bosma, Vincent Zhao, Kelvin Guu, Adams Wei Yu, Brian Lester, Nan Du, Andrew M. Dai, and Quoc V Le. Finetuned language models are zero-shot learners. In *The Tenth International Conference on Learning Representations*, 2022.
- [55] Yuxiang Wei, Zhe Wang, Jiawei Liu, Yifeng Ding, and Lingming Zhang. Magicoder: Empowering code generation with OSS-Instruct. In *Proceedings of the 41st International Conference on Machine Learning*. PMLR, 2024.
- [56] Johannes Welbl, Nelson F. Liu, and Matt Gardner. Crowdsourcing multiple choice science questions. In *Proceedings of the 3rd Workshop on Noisy User-generated Text*, pages 94–106, 2017.
- [57] Adina Williams, Nikita Nangia, and Samuel Bowman. A broad-coverage challenge corpus for sentence understanding through inference. In *Proceedings of the 2018 Conference of the North American Chapter of the Association for Computational Linguistics: Human Language Technologies, Volume 1 (Long Papers)*. Association for Computational Linguistics, 2018.
- [58] Xun Wu, Shaohan Huang, and Furu Wei. Mixture of LoRA experts. In *The Twelfth International Conference on Learning Representations*, 2024.
- [59] Longhui Yu, Weisen Jiang, Han Shi, Jincheng YU, Zhengying Liu, Yu Zhang, James Kwok, Zhenguo Li, Adrian Weller, and Weiyang Liu. Metamath: Bootstrap your own mathematical questions for large language models. In *The Twelfth International Conference on Learning Representations*, 2024.
- [60] Xiang Yue, Xingwei Qu, Ge Zhang, Yao Fu, Wenhao Huang, Huan Sun, Yu Su, and Wenhua Chen. Mammoth: Building math generalist models through hybrid instruction tuning. In *The Twelfth International Conference on Learning Representations*, 2024.
- [61] Rowan Zellers, Ari Holtzman, Yonatan Bisk, Ali Farhadi, and Yejin Choi. Hellaswag: Can a machine really finish your sentence? In *Proceedings of the 57th Annual Meeting of the Association for Computational Linguistics*, 2019.
- [62] Qingru Zhang, Minshuo Chen, Alexander Bukharin, Nikos Karampatziakis, Pengcheng He, Yu Cheng, Weizhu Chen, and Tuo Zhao. AdaLoRA: Adaptive budget allocation for parameter-efficient fine-tuning. In *The Eleventh International Conference on Learning Representations*, 2023.

Appendix

I Complete details of the motivating example

This appendix gives the full derivation for the linear-regression example in Section 2. The purpose of the toy example is to isolate the structural limitation of a fixed, input-independent correction: the same update is applied both to inputs requiring adaptation and to inputs whose pretrained behavior should be preserved

Setup. Let $\mathbf{W}_0 \in \mathbb{R}^{d \times d}$ be the frozen pre-trained linear map. Inputs are sampled from the symmetric mixture of a fine-tuning population p_{ft} and a pre-training population p_{pt} :

$$\mathbf{x} \sim \begin{cases} p_{\text{ft}} & \text{w.p. } \frac{1}{2}, \\ p_{\text{pt}} & \text{w.p. } \frac{1}{2}. \end{cases} \quad (10)$$

The target is

$$\mathbf{y} = \begin{cases} (\mathbf{W}_0 + \mathbf{M})\mathbf{x} & \text{when } \mathbf{x} \sim p_{\text{ft}}, \\ \mathbf{W}_0\mathbf{x} & \text{when } \mathbf{x} \sim p_{\text{pt}}, \end{cases} \quad (11)$$

where $\mathbf{M} \in \mathbb{R}^{d \times d}$ is the task-specific update. Thus the desired correction is $\mathbf{M}\mathbf{x}$ on fine-tuning inputs and $\mathbf{0}$ on pre-training inputs.

I.1 The best fixed correction

Consider any fixed matrix correction $\Delta \in \mathbb{R}^{d \times d}$. After subtracting the frozen term $\mathbf{W}_0\mathbf{x}$ from both the model and the target, the population loss is

$$\mathcal{L}(\Delta) = \frac{1}{2} \mathbb{E}_{p_{\text{ft}}} \left[\|\Delta - \mathbf{M}\|_2^2 \right] + \frac{1}{2} \mathbb{E}_{p_{\text{pt}}} \left[\|\Delta\|_2^2 \right]. \quad (12)$$

Let

$$\Sigma_{\mathbf{xx}}^{\text{ft}} := \mathbb{E}_{p_{\text{ft}}} [\mathbf{xx}^\top], \quad \Sigma_{\mathbf{xx}}^{\text{pt}} := \mathbb{E}_{p_{\text{pt}}} [\mathbf{xx}^\top] \quad (13)$$

denote the uncentered second-moment matrices. Then

$$\mathcal{L}(\Delta) = \frac{1}{2} \text{Tr}((\Delta - \mathbf{M})\Sigma_{\mathbf{xx}}^{\text{ft}}(\Delta - \mathbf{M})^\top) + \frac{1}{2} \text{Tr}(\Delta\Sigma_{\mathbf{xx}}^{\text{pt}}\Delta^\top). \quad (14)$$

Taking the derivative with respect to Δ gives

$$\nabla_{\Delta} \mathcal{L} = (\Delta - \mathbf{M})\Sigma_{\mathbf{xx}}^{\text{ft}} + \Delta\Sigma_{\mathbf{xx}}^{\text{pt}}. \quad (15)$$

Assuming $\Sigma_{\mathbf{xx}}^{\text{ft}} + \Sigma_{\mathbf{xx}}^{\text{pt}}$ is invertible, the unconstrained fixed-correction minimizer satisfies

$$\Delta_{\text{uncon}}^* = \mathbf{M}\Sigma_{\mathbf{xx}}^{\text{ft}}(\Sigma_{\mathbf{xx}}^{\text{ft}} + \Sigma_{\mathbf{xx}}^{\text{pt}})^{-1}. \quad (16)$$

Suppose the two populations have the same uncentered second moment:

$$\Sigma_{\mathbf{xx}}^{\text{ft}} = \Sigma_{\mathbf{xx}}^{\text{pt}} =: \Sigma_{\mathbf{xx}}. \quad (17)$$

Then we have:

$$\Delta_{\text{uncon}}^* = \frac{1}{2}\mathbf{M}. \quad (18)$$

Substituting this back into (12),

$$\begin{aligned} \mathcal{L}(\Delta_{\text{uncon}}^*) &= \frac{1}{2} \mathbb{E}_{p_{\text{ft}}} \left[\left\| -\frac{1}{2}\mathbf{M}\mathbf{x} \right\|_2^2 \right] + \frac{1}{2} \mathbb{E}_{p_{\text{pt}}} \left[\left\| \frac{1}{2}\mathbf{M}\mathbf{x} \right\|_2^2 \right] \\ &= \frac{1}{8} \mathbb{E}_{p_{\text{ft}}} \left[\|\mathbf{M}\mathbf{x}\|_2^2 \right] + \frac{1}{8} \mathbb{E}_{p_{\text{pt}}} \left[\|\mathbf{M}\mathbf{x}\|_2^2 \right] \\ &= \frac{1}{4} \mathbb{E}_{\mathbf{x} \sim \frac{1}{2}p_{\text{ft}} + \frac{1}{2}p_{\text{pt}}} \left[\|\mathbf{M}\mathbf{x}\|_2^2 \right] \\ &= \frac{1}{4} \text{Tr}(\mathbf{M}\Sigma_{\mathbf{xx}}\mathbf{M}^\top). \end{aligned} \quad (19)$$

$$= \frac{1}{4} \text{Tr}(\mathbf{M}\Sigma_{\mathbf{xx}}\mathbf{M}^\top). \quad (20)$$

This shows the tradeoff: the best fixed correction applies only half of the desired update on p_{ft} and applies a nonzero half-update on p_{pt} .

I.2 The Bayes-optimal input-dependent correction

Now allow the correction to be any measurable function $f : \mathbb{R}^d \rightarrow \mathbb{R}^d$. The loss becomes

$$\mathcal{L}(f) = \frac{1}{2} \mathbb{E}_{p_{\text{ft}}} \left[\|f(\mathbf{x}) - \mathbf{M}\mathbf{x}\|_2^2 \right] + \frac{1}{2} \mathbb{E}_{p_{\text{pt}}} \left[\|f(\mathbf{x})\|_2^2 \right]. \quad (21)$$

Writing the expectations as integrals, the contribution of a fixed input \mathbf{x} is

$$J_{\mathbf{x}}(v) = \frac{1}{2} p_{\text{ft}}(\mathbf{x}) \|v - \mathbf{M}\mathbf{x}\|_2^2 + \frac{1}{2} p_{\text{pt}}(\mathbf{x}) \|v\|_2^2, \quad (22)$$

where $v = f(\mathbf{x})$. Since $J_{\mathbf{x}}$ depends on f only through its value at \mathbf{x} , the optimal function is obtained by minimizing this quadratic separately for each \mathbf{x} .

The first-order condition is

$$p_{\text{ft}}(\mathbf{x})(v - \mathbf{M}\mathbf{x}) + p_{\text{pt}}(\mathbf{x})v = 0, \quad (23)$$

so the Bayes-optimal correction is

$$f^*(\mathbf{x}) = \pi_{\text{ft}}(\mathbf{x})\mathbf{M}\mathbf{x}, \quad \pi_{\text{ft}}(\mathbf{x}) := \frac{p_{\text{ft}}(\mathbf{x})}{p_{\text{ft}}(\mathbf{x}) + p_{\text{pt}}(\mathbf{x})}. \quad (24)$$

Here $\pi_{\text{ft}}(\mathbf{x})$ is the posterior probability that \mathbf{x} came from the fine-tuning population under the symmetric mixture. The corresponding Bayes loss is

$$\mathcal{L}_{\text{Bayes}} = \frac{1}{2} \int \frac{p_{\text{ft}}(\mathbf{x})p_{\text{pt}}(\mathbf{x})}{p_{\text{ft}}(\mathbf{x}) + p_{\text{pt}}(\mathbf{x})} \|\mathbf{M}\mathbf{x}\|_2^2 d\mathbf{x}. \quad (25)$$

No input-dependent method can achieve a smaller squared-error loss on this population problem, because (24) is the pointwise minimizer of the loss integrand.

I.3 DISeL realizes the Bayes predictor

Assume that the two populations are multivariate Gaussian with the same covariance matrix but different means:

$$p_{\text{ft}}(\mathbf{x}) = \mathcal{N}(\mathbf{x}; \boldsymbol{\mu}_{\text{ft}}, \boldsymbol{\Sigma}), \quad p_{\text{pt}}(\mathbf{x}) = \mathcal{N}(\mathbf{x}; \boldsymbol{\mu}_{\text{pt}}, \boldsymbol{\Sigma}). \quad (26)$$

Then we can compute the Bayes-optimal correction exactly as follows:

$$\begin{aligned} \log \frac{p_{\text{ft}}(\mathbf{x})}{p_{\text{pt}}(\mathbf{x})} &= -\frac{1}{2}(\mathbf{x} - \boldsymbol{\mu}_{\text{ft}})^\top \boldsymbol{\Sigma}^{-1}(\mathbf{x} - \boldsymbol{\mu}_{\text{ft}}) + \frac{1}{2}(\mathbf{x} - \boldsymbol{\mu}_{\text{pt}})^\top \boldsymbol{\Sigma}^{-1}(\mathbf{x} - \boldsymbol{\mu}_{\text{pt}}) \\ &= (\boldsymbol{\mu}_{\text{ft}} - \boldsymbol{\mu}_{\text{pt}})^\top \boldsymbol{\Sigma}^{-1} \mathbf{x} - \frac{1}{2}(\boldsymbol{\mu}_{\text{ft}}^\top \boldsymbol{\Sigma}^{-1} \boldsymbol{\mu}_{\text{ft}} - \boldsymbol{\mu}_{\text{pt}}^\top \boldsymbol{\Sigma}^{-1} \boldsymbol{\mu}_{\text{pt}}) \\ &:= \mathbf{w}_g^\top \mathbf{x} + b_g, \end{aligned} \quad (27)$$

where

$$\mathbf{w}_g := \boldsymbol{\Sigma}^{-1}(\boldsymbol{\mu}_{\text{ft}} - \boldsymbol{\mu}_{\text{pt}}) \in \mathbb{R}^d, \quad b_g := \frac{1}{2}(\boldsymbol{\mu}_{\text{pt}}^\top \boldsymbol{\Sigma}^{-1} \boldsymbol{\mu}_{\text{pt}} - \boldsymbol{\mu}_{\text{ft}}^\top \boldsymbol{\Sigma}^{-1} \boldsymbol{\mu}_{\text{ft}}) \in \mathbb{R}. \quad (28)$$

Substituting (27) into (24), we have

$$\pi_{\text{ft}}(\mathbf{x}) = \frac{p_{\text{ft}}(\mathbf{x})}{p_{\text{ft}}(\mathbf{x}) + p_{\text{pt}}(\mathbf{x})} = \frac{1}{1 + \exp(-(\mathbf{w}_g^\top \mathbf{x} + b_g))} = \sigma(\mathbf{w}_g^\top \mathbf{x} + b_g), \quad (29)$$

and thus the Bayes-optimal correction is a sigmoid gate multiplying the task update:

$$f^*(\mathbf{x}) = \sigma(\mathbf{w}_g^\top \mathbf{x} + b_g) \mathbf{M}\mathbf{x}. \quad (30)$$

Choice of DISeL parameters that realize f^* . Given any factorization $\mathbf{M} = \mathbf{A}\mathbf{B}$ with $\mathbf{A} \in \mathbb{R}^{d \times r}$ and $\mathbf{B} \in \mathbb{R}^{r \times d}$ (which exists whenever $\text{rank}(\mathbf{M}) \leq r$), set the gate parameters to

$$\mathbf{W}_g = \mathbf{1}_r \mathbf{w}_g^\top \in \mathbb{R}^{r \times d}, \quad \mathbf{b}_g = b_g \mathbf{1}_r \in \mathbb{R}^r, \quad (31)$$

where $\mathbf{1}_r = (1, \dots, 1)^\top \in \mathbb{R}^r$ and \mathbf{w}_g, b_g are given by (28). Each rank's gate then takes the same value

$$g_i(\mathbf{x}) = \sigma(\mathbf{w}_g^\top \mathbf{x} + b_g) = \pi_{\text{ft}}(\mathbf{x}), \quad i = 1, \dots, r, \quad (32)$$

so $\mathbf{G}(\mathbf{x}) = \pi_{\text{ft}}(\mathbf{x}) \mathbf{I}_r$ and the DISeL correction is

$$\mathbf{A} \mathbf{G}(\mathbf{x}) \mathbf{B} \mathbf{x} = \pi_{\text{ft}}(\mathbf{x}) \mathbf{A} \mathbf{B} \mathbf{x} = \pi_{\text{ft}}(\mathbf{x}) \mathbf{M} \mathbf{x} = f^*(\mathbf{x}). \quad (33)$$

Hence DISeL represents the Bayes-optimal input-dependent correction exactly in this case.

I.4 Experimental setup for Figure 1

For the concrete experiment, we use $d = 16$. $\mathbf{M} = \mathbf{UV}$ with $\mathbf{U} \in \mathbb{R}^{d \times 2}$ and $\mathbf{V} \in \mathbb{R}^{2 \times d}$ sampled with i.i.d. standard Gaussian entries, so $\text{rank}(\mathbf{M}) = 2$ almost surely. We write $\mathbf{x} = (x_1, \mathbf{x}_{2:d})$ and use

$$p_{\text{ft}} : x_1 \sim \mathcal{N}(+\mu, s^2), \quad \mathbf{x}_{2:d} \sim \mathcal{N}(\mathbf{0}, \mathbf{I}_{d-1}), \quad (34)$$

$$p_{\text{pt}} : x_1 \sim \mathcal{N}(-\mu, s^2), \quad \mathbf{x}_{2:d} \sim \mathcal{N}(\mathbf{0}, \mathbf{I}_{d-1}), \quad (35)$$

with $\mu = 3$ and $s^2 = 0.25$. The two populations differ only in the sign of the mean of x_1 .

Since the experiment uses LORA rank $r = 2$ and $\text{rank}(\mathbf{M}) = 2$, the matrix $\frac{1}{2}\mathbf{M}$ is feasible for rank-2 LORA. Hence, in this toy example, the rank-constrained LORA optimum is exactly the unconstrained fixed-correction optimum in (18). The loss in (20) is therefore not only a lower bound; it is the actual best loss achievable by a fixed rank-2 correction.

II ROBERTa experiments: details and hyperparameters

This appendix provides the full setup for the ROBERTa-base experiments on five GLUE tasks reported in Section 4.1 of the main paper.

II.1 Model and tasks

Architecture. We use ROBERTa-base [29] (125M parameters) initialized from the HuggingFace roberta-base checkpoint. Each task uses a randomly initialized linear classification head trained jointly with the adapter.

Adapter target modules. All adapters (and Full FT, when applicable) act on every linear layer in the encoder:

- Attention: `q_proj, k_proj, v_proj, attention.output.dense`.
- MLP: `intermediate.dense, output.dense`.

Tasks. Five GLUE tasks [47]: MNLI, SST-2, QNLI, CoLA, and MRPC. The underlying task datasets are MULTINLI, SST, SQUAD-derived QNLI, CoLA, and MRPC [12, 39, 43, 53, 57]; sample counts and per-task validation metrics are listed in Table 1. Validation accuracy is reported per task; the headline score is their unweighted mean.

Table 1: The five GLUE tasks used for fine-tuning ROBERTa-base.

Task	# train	# classes	Validation metric
MNLI	392,702	3	matched accuracy
SST-2	67,349	2	accuracy
QNLI	104,743	2	accuracy
CoLA	8,551	2	accuracy
MRPC	3,668	2	accuracy

CoLA reports accuracy rather than Matthews correlation so that all five tasks share a metric on the same scale, making the cross-task average meaningful.

II.2 Methods compared

At every rank $r \in \{4, 8, 16, 32, 64\}$ we train four parameter-efficient methods: LORA [19], DoRA [28], ADALORA [62] (target rank r , initial rank $2r$), and DISeL. The four methods share the same target modules, optimizer, schedule, batch size, sequence length, and number of epochs (Table 2); they differ only in the per-method configuration listed in the next subsection. We additionally train Full FT — the entire encoder plus classification head — as an upper-bound reference; it is not a competing PEFT method, and its per-task hyperparameters are listed separately in Table 4. Each

(method, task, rank) cell is run with three seeds; the points in Figure 2 are across-seed means with standard-deviation error bars.

II.3 Common training hyperparameters

The following are shared across all methods, tasks, and ranks unless explicitly overridden below.

Table 2: Common training hyperparameters shared across all methods, tasks, and ranks.

Hyperparameter	Value
<i>Optimization</i>	
Optimizer	AdamW ($\beta_1=0.9, \beta_2=0.999, \epsilon=10^{-8}$)
Weight decay	0.01
Max gradient norm	1.0
<i>Learning-rate schedule</i>	
Scheduler	cosine
Warmup ratio	0.02
<i>Batch and sequence</i>	
Per-device batch size	8
Gradient accumulation	2
Effective batch size	16
Max sequence length	512
<i>Precision and hardware</i>	
Precision	bfloat16 mixed precision
GPUs per run	1
<i>Adapter and training duration</i>	
LORA dropout	0.0
Epochs (adapter methods)	15
Epochs (Full FT)	5 on MNLI/QNLI/SST-2; 10 on CoLA/MRPC

II.4 Method-specific hyperparameters

Rank-scaled learning rate (LORA, DORA, and the LORA branch of DISeL). For these three methods we scale the learning rate with the adapter rank following Shuttleworth et al. [42].

ADALORA. We set the initial rank to $\text{init}_r = 2r$ and prune in a single step to the target rank r . The pruning step is chosen per task, roughly in proportion to the training-set size, giving 37k for MNLI, 10k for QNLI, 6k for SST-2, 800 for CoLA, and 350 for MRPC (so $t_{\text{init}} = t_{\text{final}}$). The remaining knobs follow the PEFT defaults: $\Delta_t = 10$, $\alpha = 2r$, and orthogonality-regularization weight 0.5. The learning rate is held at 8×10^{-4} for every task and rank.

DISeL gate hyperparameters. The gate parameters ($\mathbf{W}_g, \mathbf{b}_g$) are trained jointly with the LORA factors (\mathbf{A}, \mathbf{B}). The LORA path uses the rank-scaled learning rate, and the gate uses a separate, larger one. We initialize \mathbf{W}_g with the PEFT default (scaled orthogonal initialization) and tune the gate bias \mathbf{b}_g and gate learning rate per task; ties on validation accuracy are broken in favor of the configuration with lower forgetting.

CoLA and MRPC use a larger gate learning rate because their training sets are relatively small. With $\text{gate_lr} = 10^{-4}$, the gates remain close to their near-closed initialization, leading to under-training of the LORA path and reduced accuracy. Increasing the gate learning rate to 10^{-3} , together with a less negative bias, allows the gates to activate more readily and yields competitive performance. In contrast, for MNLI, QNLI, and SST-2, the smaller gate learning rate is sufficient and results in lower forgetting. A summary is provided in Table 3.

Table 3: Per-task DISeL gate hyperparameters.

Task	Gate bias init \mathbf{b}_g	Gate LR
MNLI	$-7 \cdot \mathbf{1}$ (uniform across ranks)	1×10^{-4}
SST-2	$-7 \cdot \mathbf{1}$	1×10^{-4}
QNLI	$-7 \cdot \mathbf{1}$	1×10^{-4}
CoLA	-3 at $r \in \{4, 16, 32\}$; -7 at $r \in \{8, 64\}$	1×10^{-3}
MRPC	-3 at $r \in \{4, 16\}$; -7 at $r \in \{8, 32\}$; -5 at $r=64$	1×10^{-3}

Full FT (reference upper bound). No adapter is used; every encoder parameter and the classification head are trained jointly. All other training hyperparameters match the adapter runs. Per-task LR and epoch count can be found in Table 4.

Table 4: Full FT per-task hyperparameters.

Task	Learning rate	Epochs
MNLI	1×10^{-5}	5
QNLI	1×10^{-5}	5
SST-2	1×10^{-5}	5
CoLA	2×10^{-5}	10
MRPC	2×10^{-5}	10

II.5 Evaluation protocol

Best-checkpoint selection. We go over all the checkpoints we saved during training and pick the one with the best fine-tuning accuracy. The forgetting accuracy is also measured on this checkpoint.

Fine-tuning score (y-axis of Figure 2). For each (method, rank, seed), the fine-tuning score is the unweighted mean of the five per-task validation accuracies,

$$\text{FT score} = \frac{1}{5}(\text{MNLI}_{\text{acc}} + \text{SST-2}_{\text{acc}} + \text{CoLA}_{\text{acc}} + \text{QNLI}_{\text{acc}} + \text{MRPC}_{\text{acc}}). \quad (36)$$

Forgetting score (x-axis of Figure 2). We measure forgetting as masked-LM perplexity on three held-out corpora. After fine-tuning, the encoder is paired with the original ROBERTa MLM head and evaluated on WIKITEXT-2 (HuggingFace `wikitext`, `wikitext-2-raw-v1`, validation split), BOOKCORPUSOPEN (`bookcorpusopen`), and CC-NEWS (`cc_news`); for the latter two we sample 10k sentences with a fixed seed. The figure plots the average of the three perplexities on a log scale. For reference, the pre-trained checkpoint scores 7.64, 5.94, and 5.63 on the three corpora ($\text{ppl}_{\text{base}} \approx 6.40$ overall).

II.6 Infrastructure

Each run uses a single NVIDIA A100 (40GB) GPU. We implement experiments in Python 3.13.5 with PyTorch (CUDA 13), using the HuggingFace `transformers`, `peft`, and `datasets` libraries, as well as the `lm-evaluation-harness`.

III LLAMA and MISTRAL Experiments: Details and Hyperparameters

In this section, we provide the full setup for the LLM experiments reported in Section 4.2.

III.1 Models and training data

We fine-tune two open-weight 7B causal language models on two instruction-tuning corpora; the pairing of base model, corpus, sample count, and prompt template are summarized in Table 5.

Table 5: Base models and instruction-tuning corpora.

Setting	Base model	#training samples	Prompt template
Math	LLAMA 2-7B [46] (Llama-2-7b-hf)	~ 395K	Alpaca
Code	MISTRAL-7B [21] (Mistral-7B-v0.1)	~ 110K	Magicode

The math corpus is METAMATHQA [59]; the code corpus is MAGICODER-EVOL-INSTRUCT-110K [55]. Loss is computed only on response tokens; the instruction prefix is masked. We hold out a 5% random validation split (seed 42) and train on the remaining 95%. We do not perform validation-loss-based early stopping; every saved checkpoint is evaluated on the downstream benchmarks (Section III.6).

Prompt templates. The math runs use the standard Alpaca template:

```
### Instruction:
{instruction}
```

```
### Response:
{output}
```

The code runs use the Magicode template:

```
You are an exceptionally intelligent coding assistant that consistently delivers
accurate and reliable responses to user instructions.
```

```
@@ Instruction
{instruction}
```

```
@@ Response
{output}
```

III.2 Common training hyperparameters

The following are shared across all methods, ranks, and seeds for both LLAMA and MISTRAL runs unless explicitly overridden in the method-specific section below; values are listed in Table 6.

III.3 Adapter configuration

The four adapter methods (LORA, DORA, ADALORA, and DISeL) share the following baseline configuration.

- **Target modules.** Every linear projection inside the decoder blocks: q_proj, k_proj, v_proj, o_proj, gate_proj, up_proj, and down_proj. The LM head and embeddings are frozen.
- **Bias.** Not trained.
- **Adapter dropout.** 0.0.
- **Scaling.** $\alpha = 2r$.
- **Initialization.** The LORA factor \mathbf{A} is Kaiming-uniform, $\mathbf{B} = \mathbf{0}$.

III.4 Method-specific hyperparameters

LORA. Standard LORA [19] as implemented in HuggingFace `peft`: for each pre-trained weight $\mathbf{W} \in \mathbb{R}^{d_y \times d_x}$ in the target set, we learn $\Delta = \frac{\alpha}{r} \mathbf{A} \mathbf{B}$ with $\mathbf{A} \in \mathbb{R}^{d_y \times r}$ and $\mathbf{B} \in \mathbb{R}^{r \times d_x}$, matching the notation of Section 3.

Table 6: Training hyperparameters shared across all methods, ranks, and seeds.

Hyperparameter	Value
<i>Optimization</i>	
Optimizer	AdamW ($\beta_1=0.9, \beta_2=0.999, \varepsilon=10^{-8}$)
Weight decay	0.01 (excluded from biases, LayerNorm, and gate parameters)
Max gradient norm	1.0
<i>Learning-rate schedule</i>	
Scheduler	cosine
Warmup ratio	0.02
<i>Batch and sequence</i>	
Effective batch size	32 sequences per optimizer step
Max sequence length	512 (math) / 2048 (code)
<i>Precision and hardware</i>	
Precision	bfloat16
Gradient checkpointing	enabled
GPUs per run	4× NVIDIA A100 (40 GB), data-parallel
<i>Training duration</i>	
Epochs	3
Checkpoints saved	2 per epoch (cap 16, oldest pruned)

ADALORA. We use the original recipe of Zhang et al. [62] via HuggingFace `peft`, with initial rank $\text{init}_r = 1.5r$ and the budget-reduction schedule of the paper’s SQUAD setting (warm-up to $t_{\text{init}} \approx 17\%$ of total steps, pruning ending at $t_{\text{final}} \approx 33\%$, $\Delta_t = 10$, $\beta_1 = \beta_2 = 0.85$); per-setting step counts are given in Table 7. We set the orthogonality-regularization weight to 0.1, again following the original paper, since the PEFT default of 0.5 dominated the training loss in pilot runs. All other adapter settings ($\alpha = 2r$, dropout, target modules) match LORA. The learning rate is 2×10^{-4} for $r \in \{16, 32, 64, 128\}$ and 1×10^{-4} for $r = 256$ to avoid divergence at $\text{init}_r = 384$.

Table 7: ADALORA budget-reduction schedule per setting. All ranks within a setting share the same total step count.

Setting	Total steps	t_{init}	t_{final}
LLAMA 2 7B / METAMATHQA	8 796	1 574	3 055
MISTRAL 7B / MAGICODER	2 478	420	820

Full FT. All transformer parameters are unfrozen ($\approx 6.74\text{B}$ for LLAMA 2 7B and $\approx 7.24\text{B}$ for MISTRAL 7B), including the LM head and the input embeddings. Two learning rates were swept (10^{-5} and 5×10^{-5}); we report 10^{-5} in the main figure (5×10^{-5} was unstable on math). All other settings (optimizer, schedule, batch size, epochs, precision, gradient checkpointing) match the adapter runs.

DISeL gate hyperparameters. For every adapted layer, an input-dependent rank gate is attached to the LORA branch:

$$\Delta(\mathbf{x}) \mathbf{x} = \frac{\alpha}{r} \mathbf{A} \mathbf{G}(\mathbf{x}) \mathbf{B} \mathbf{x}, \quad g(\mathbf{x}) = \sigma(\mathbf{W}_g \mathbf{x} + \mathbf{b}_g) \in (0, 1)^r, \quad (37)$$

with $\mathbf{W}_g \in \mathbb{R}^{r \times d_x}$, matching the notation of Section 3. The gate adds $r d_x + r$ parameters per adapted layer. The remaining gate-specific hyperparameters (bias and weight initialization, gate normalization, gate learning rate, target modules) are listed in Table 8.

Table 8: DISeL gate hyperparameters used for both LLAMA and MISTRAL.

Gate hyperparameter	Value
Bias init \mathbf{b}_g	-3.0 ($\sigma(-3) \approx 0.047$, gates start nearly closed)
Weight init \mathbf{W}_g	Kaiming-uniform
Gate normalization	off
Gate learning rate	10^{-3} (separate AdamW group; weight decay disabled)
Targets	identical to LoRA

III.5 Per-rank learning rates

For every method we report the learning rate that gave the highest target-task accuracy in our sweep over $\{10^{-4}, 2 \times 10^{-4}, 4 \times 10^{-4}\}$ for adapter methods, and $\{10^{-5}, 5 \times 10^{-5}, 10^{-4}\}$ for Full FT. The effective batch size is held at 32 for every run; per-device batch and gradient-accumulation count are adjusted at the largest ranks (down to per-device 2×16 for MISTRAL DISeL at $r=256$) to fit GPU memory. The selected learning rates for every (method, rank, setting) cell are summarized in Table 9.

Table 9: Per-run learning rates for both fine-tuning settings.

Method	Rank r	LLAMA 2 7B (math)	MISTRAL 7B (code)
LoRA	16	2×10^{-4}	2×10^{-4}
LoRA	32	2×10^{-4}	2×10^{-4}
LoRA	64	2×10^{-4}	1×10^{-4}
LoRA	128	2×10^{-4}	2×10^{-4}
LoRA	256	1×10^{-4}	1×10^{-4}
DoRA	16	2×10^{-4}	2×10^{-4}
DoRA	32	2×10^{-4}	2×10^{-4}
DoRA	64	2×10^{-4}	2×10^{-4}
DoRA	128	2×10^{-4}	2×10^{-4}
DoRA	256	1×10^{-4}	1×10^{-4}
ADALoRA	16	2×10^{-4}	2×10^{-4}
ADALoRA	32	2×10^{-4}	2×10^{-4}
ADALoRA	64	2×10^{-4}	2×10^{-4}
ADALoRA	128	2×10^{-4}	2×10^{-4}
ADALoRA	256	1×10^{-4}	1×10^{-4}
DISeL	16	2×10^{-4}	2×10^{-4}
DISeL	32	2×10^{-4}	2×10^{-4}
DISeL	64	2×10^{-4}	2×10^{-4}
DISeL	128	2×10^{-4}	2×10^{-4}
DISeL	256	1×10^{-4}	1×10^{-4}
Full FT	no adapter	1×10^{-5}	1×10^{-5}

III.6 Evaluation protocol

All evaluation runs use a single A100 GPU with bfloat16 inference. The adapter is *not* merged into the base weights: the PEFT model is loaded in evaluation mode with all adapter parameters and (for DISeL) the gate parameters restored from disk.

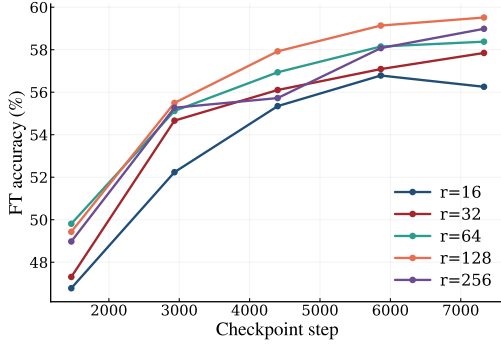
Target-task evaluation.

- **Math (LLAMA 2 7B / METAMATHQA):** GSM8K, 5-shot, exact_match, strict-match.
- **Code (MISTRAL 7B / MAGICODER):** HUMAN EVAL pass@1 with greedy decoding, one sample per problem (164 problems).

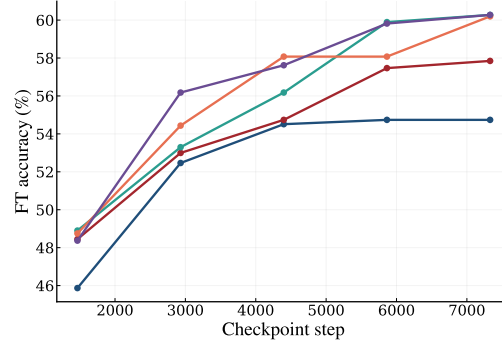
Forgetting suite (both settings). The retention score reported in the main figure is the unweighted mean accuracy across the 14 benchmarks listed in Table 10, all evaluated 5-shot under the same lm-eval configuration with max_length=512. The same suite is used for both math and code runs.

Table 10: Forgetting (retention) suite: 14 benchmarks evaluated 5-shot under the same lm-eval configuration for both LLAMA (math) and MISTRAL (code) runs.

Benchmark	Category	Metric
HELLASWAG [61]	Commonsense reasoning	acc_norm
WINOGRANDE [41]	Commonsense reasoning	acc
ARC-CHALLENGE [8]	Science QA	acc_norm
ARC-EASY [8]	Science QA	acc_norm
LAMBADA-OPENAI [38]	Language modeling	acc (and perplexity)
BOOLQ [7]	Reading comprehension	acc
PIQA [3]	Physical commonsense	acc_norm
TRIVIAQA [24]	Open-domain QA	acc
OPENBOOKQA [36]	Science QA	acc_norm
SCIQ [56]	Science QA	acc
MMLU (57-task aggregate) [18]	Multitask knowledge	acc
MEDQA-4OPTIONS [23]	Medical QA	acc
COMMONSENSEQA [44]	Commonsense reasoning	acc
NATURALQUESTIONS-OPEN	Open-domain QA	acc

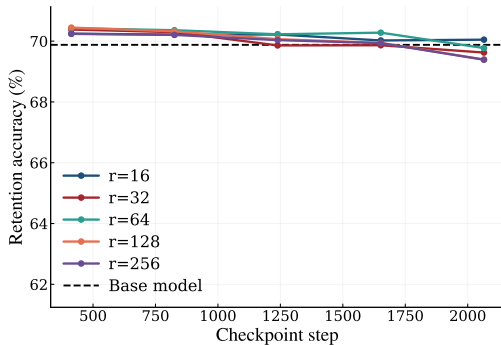


(a) **DISeL**: GSM8K accuracy improves over training across ranks.

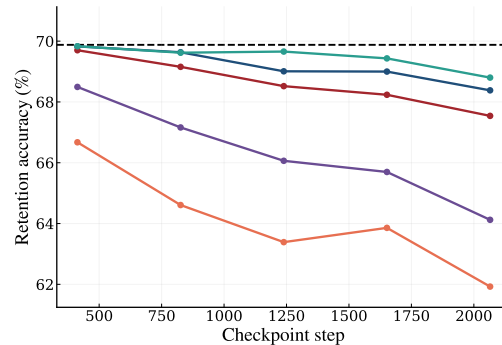


(b) **LORA**: GSM8K accuracy also improves, but retention degrades at larger ranks.

Figure 7: **Fine-tuning accuracy over training checkpoints for LORA and DISeL on LLAMA 2 7B / METAMATHQA**. Each curve reports GSM8K accuracy at every saved checkpoint, for adapter ranks $r \in \{16, 32, 64, 128, 256\}$.



(a) **DISeL**: retention stays close to the base model across ranks and training checkpoints.



(b) **LORA**: retention degrades over training, with larger drops at higher ranks.

Figure 8: **Retention over training checkpoints for LORA and DISeL on MISTRAL 7B / MAGICODER**. Each curve tracks the unweighted mean accuracy across the 14-benchmark retention suite at every saved checkpoint, for adapter ranks $r \in \{16, 32, 64, 128, 256\}$.

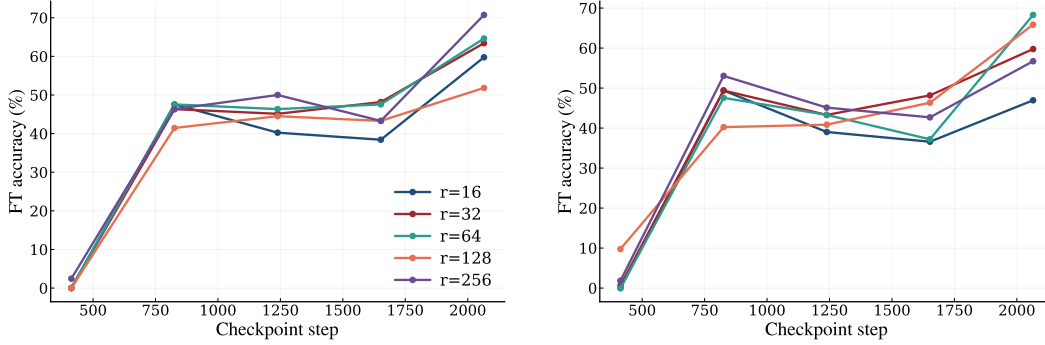
IV Checkpoint Dynamics: Retention and Fine-Tuning Accuracy

IV.1 LLAMA 2 7B / METAMATHQA

Section 6 reports the checkpoint-level retention curves for the LLAMA 2 7B / METAMATHQA run. Figure 7 shows the corresponding fine-tuning accuracy curves. Both DISeL and LORA improve on GSM8K over training, but the retention curves in Figure 6 show that DISeL achieves this without the rank-dependent retention drift observed for LORA.

IV.2 MISTRAL 7B / MAGICODER

Figures 8 and 9 repeat the checkpoint-level analysis for the MISTRAL 7B / MAGICODER code-generation run. The retention pattern mirrors the LLAMA math setting in Section 6: DISeL keeps retention close to the base model throughout training and across ranks, whereas LORA exhibits rank-dependent drift. At the same time, the fine-tuning accuracy curves show that this retention advantage does not come from under-training; DISeL reaches comparable or stronger target-task accuracy at the final checkpoints.



(a) **DISeL**: target-task accuracy improves over training and remains competitive across ranks.

(b) **LORA**: target-task accuracy also improves, but with larger retention loss at high ranks.

Figure 9: **Fine-tuning accuracy over training checkpoints for LORA and DISeL on MISTRAL 7B / MAGICODER.** Each curve reports HUMANEval pass@1 at every saved checkpoint, for adapter ranks $r \in \{16, 32, 64, 128, 256\}$.

V Interpretability: Additional Results

This appendix complements the gate-activation analysis of Section 5, which focused on LLAMA 2 7B at rank $r=32$. We report (i) additional LLAMA 2 7B results across ranks and modules, and (ii) the corresponding analysis on MISTRAL 7B fine-tuned for code generation. The setup, evaluation domains, and statistics shown (sigmoid gate values aggregated over held-out inputs) are identical to Section 5; only the model, rank, or module under inspection differs.

V.1 LLAMA 2 7B: additional ranks and modules

We extend the rank-32 analysis of Section 5 along two axes. First, we recompute the domain-conditional gate distributions (math, code, general text) at additional adapter ranks to check that the depth-band pattern reported in the main text is not specific to $r=32$. Second, we extend the per-module breakdown to the remaining linear projections in the decoder (q_proj , k_proj , o_proj , $gate_proj$), so the $v_proj / up_proj / down_proj$ comparison in Figure 5 can be read in context of the full attention and MLP stacks. The qualitative picture is the same as in the main text: math inputs reach the highest gate values, the activation is concentrated in mid-to-late layers, and within those layers, the MLP path (especially up_proj) carries most of the active capacity.

Figure 10 first aggregates the adapted projections into attention (q_proj , k_proj , v_proj , o_proj) and MLP ($gate_proj$, up_proj , $down_proj$) groups on held-out GSM8K inputs. Both groups become more active in middle and late layers, but the MLP gates are consistently more open: the mean gate value rises from about 0.31 in early layers to about 0.50 in middle and late layers, compared with about 0.15 to 0.34 for attention. Figure 11 breaks this down by projection. The largest mean activations occur in $gate_proj$, up_proj , and the attention key/query projections in later layers, while v_proj and early $down_proj$ remain mostly closed. This finer view supports the main-text conclusion that DISeL does not simply open all ranks uniformly: it concentrates capacity in specific depths and projections.

V.2 MISTRAL 7B fine-tuned on code

We repeat the diagnostics of Section 5 on MISTRAL 7B fine-tuned on MAGICODER, using held-out code inputs as the fine-tuning domain and math/general text as contrast domains. Figure 12 shows the main domain-level difference from the LLAMA math adapter. On LLAMA, math inputs are clearly more activated than code, with general text lowest. On MISTRAL fine-tuned for code, code and math are nearly indistinguishable in mean gate value: early layers give 0.128 for code and 0.141 for math, middle layers give 0.224 and 0.235, and late layers give 0.331 and 0.333. However, the histogram shape still reflects the fine-tuning domain: code inputs have the largest mass of gates that are fully open, even though math sometimes has a slightly larger mean because it has more partially open gates. General text remains lower, but the gap is smaller than in the LLAMA math setting. This suggests

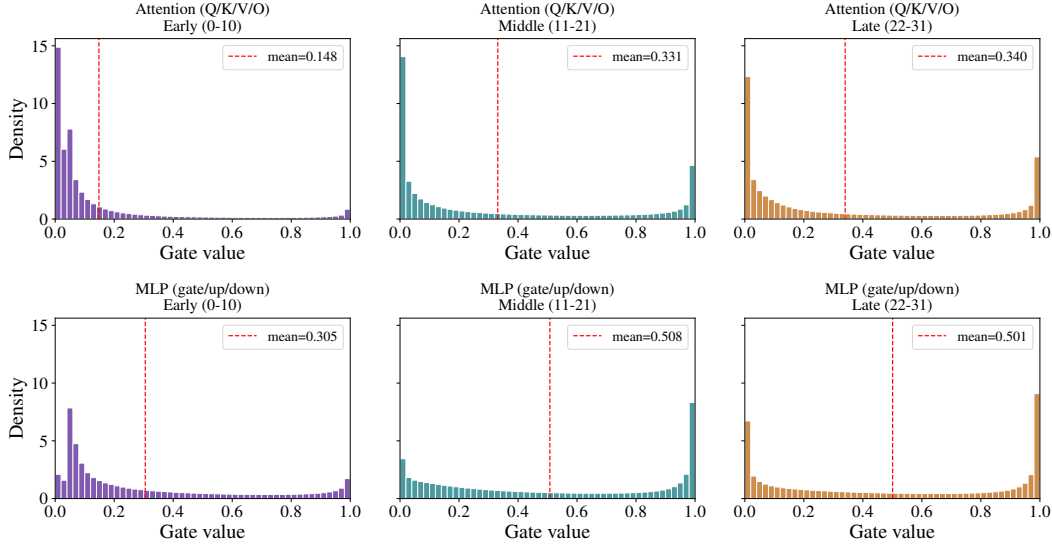


Figure 10: **Gate distributions by module family and depth on LLAMA math inputs.** We aggregate gate values from the rank-32 LLAMA math adapter over held-out GSM8K examples. Attention denotes q_{proj} , k_{proj} , v_{proj} , and o_{proj} ; MLP denotes $\text{gate}_{\text{proj}}$, up_{proj} , and $\text{down}_{\text{proj}}$. Gates open most strongly in the middle and late layers, especially in the MLP stack.

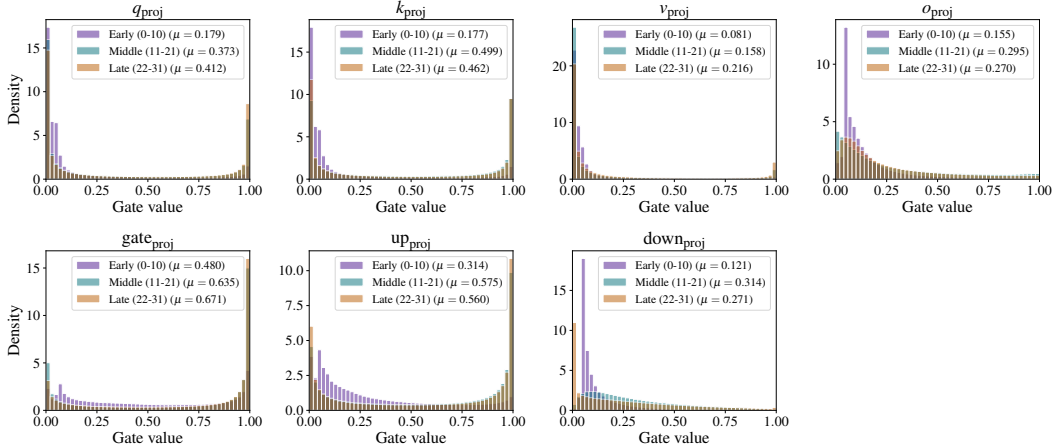


Figure 11: **Gate distributions by projection on LLAMA math inputs.** We show gate-value histograms for all adapted projections of the rank-32 LLAMA math adapter, grouped by layer-depth band. The MLP $\text{gate}_{\text{proj}}$ and up_{proj} are the most active, while v_{proj} and early $\text{down}_{\text{proj}}$ remain close to closed.

that the code adapter treats math and code as closely related structured-symbolic inputs, while still opening its highest-confidence gates most often on code.

The module-level views in Figures 13 and 14 show that the coarse organization is nevertheless similar to LLAMA. Gates open more in the middle and late layers than in the early layers, and the MLP stack is more active than the attention stack. Aggregating by module family, MLP mean activation rises from 0.211 in early layers to 0.416 in late layers, whereas attention rises from 0.066 to 0.267. The per-projection breakdown shows the strongest activations in $\text{gate}_{\text{proj}}$ and up_{proj} , with $\text{gate}_{\text{proj}}$ reaching the largest late-layer mean ($\mu \approx 0.686$). Thus, while the domain selectivity differs from LLAMA—code and math open the gates almost equally on MISTRAL—the layer and module selectivity remains consistent.

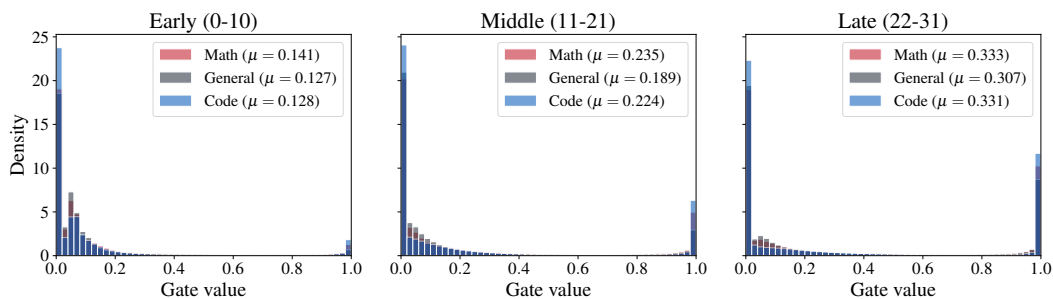


Figure 12: **Gate activation histograms across domains for the MISTRAL code adapter.** We analyze the rank-32 MISTRAL adapter fine-tuned on MAGICODER. Unlike the LLAMA math adapter, where math is clearly separated from code, the MISTRAL code adapter opens gates to a similar degree on held-out code and math inputs, while general text remains lower. Code nevertheless has the largest concentration of fully open gates, even when math has a comparable or slightly higher mean gate value.

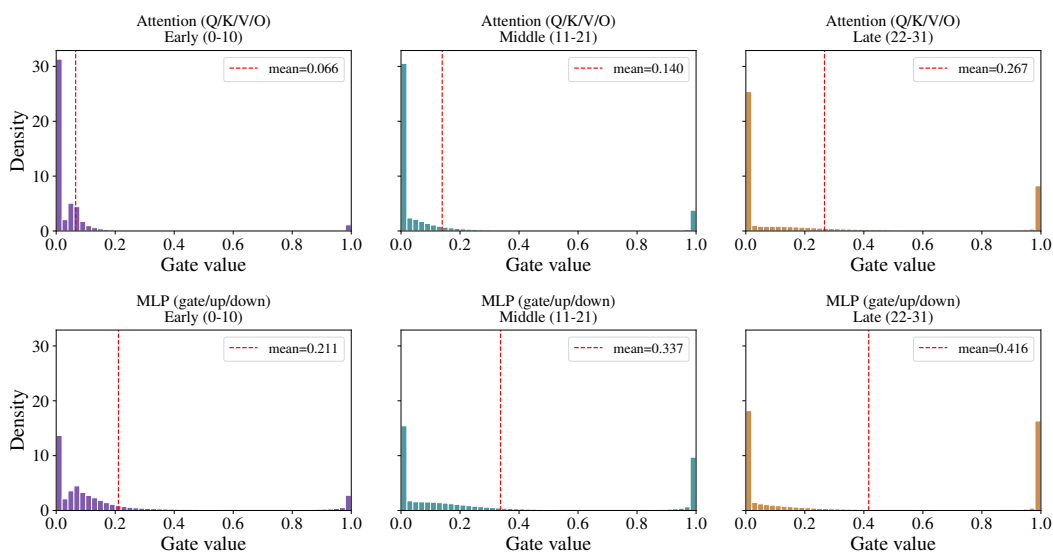


Figure 13: **Gate distributions by module family and depth on MISTRAL code inputs.** Attention denotes q_proj , k_proj , v_proj , and o_proj ; MLP denotes $gate_proj$, up_proj , and $down_proj$. As in the LLAMA analysis, gates open most strongly in the MLP stack and in middle-to-late layers.

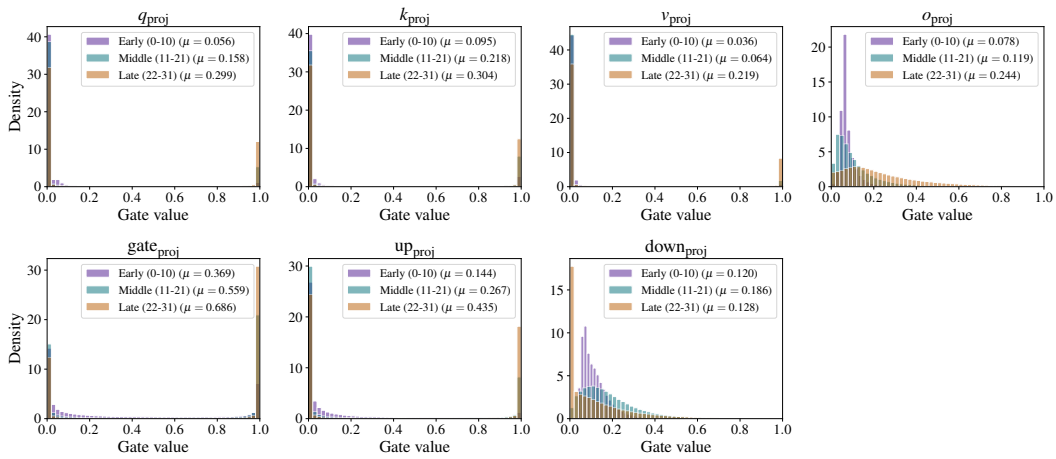


Figure 14: **Gate distributions by projection on MISTRAL code inputs.** We show gate-value histograms for all adapted projections of the rank-32 MISTRAL code adapter, grouped by layer-depth band. The largest activations occur in the MLP $gate_{proj}$ and up_{proj} , while several attention projections remain mostly closed until late layers.